SANDIA REPORT

SAND2005-7427
Unlimited Release
Printed December 2005

Predictions Of Flow Through An Isothermal Serpentine Passage With Linear Eddy-Viscosity Reynolds Averaged Navier-Stokes Models

Gregory M. Laskowski

Prepared by
Sandia National Laboratories
Albuquerque, New Mexico 87185 and Livermore, California 94550

Sandia is a multiprogram laboratory operated by Sandia Corporation,
a Lockheed Martin Company, for the United States Department of Energy's
National Nuclear Security Administration under Contract DE-AC04-94-AL85000.

Sandia National Laboratories

Issued by Sandia National Laboratories, operated for the United States Department of Energy by Sandia Corporation.

Available to DOE and DOE contractors from
U.S. Department of Energy
Office of Scientific and Technical Information
P.O. Box 62
Oak Ridge, TN 37831

Telephone: (865) 576-8401
Facsimile: (865) 576-5728
E-Mail: reports@adonis.osti.gov
Online ordering: http://www.doe.gov/bridge

Available to the public from
U.S. Department of Commerce
National Technical Information Service
5285 Port Royal Rd
Springfield, VA 22161

Telephone: (800) 553-6847
Facsimile: (703) 605-6900
E-Mail: orders@ntis.fedworld.gov
Online order: http://www.ntis.gov/help/ordermethods.asp?loc=7-4-0#online

SAND2005-7427
Unlimited Release
Printed December 2005

Predictions of Flow Through An Isothermal Serpentine Passage With Linear Eddy-Viscosity Reynolds Averaged Navier Stokes Models

Gregory M. Laskowski
Engineering Sciences and Technologies Department 8775
Sandia National Laboratories
P.O. Box 969 MS9409
Livermore, CA 94551-9409

ABSTRACT

Flows with strong curvature present a challenge for turbulence models, specifically eddy viscosity type models which assume isotropy and a linear and instantaneous equilibrium relation between stress and strain. Results obtained from three different codes and two different linear eddy viscosity turbulence models are compared to a DNS simulation in order to gain some perspective on the turbulence modeling capability of SIERRA/Fuego. The Fuego v2f results are superior to the more common two-layer k-ε model results obtained with both a commercial and research code in terms of the concave near wall behavior predictions. However, near the convex wall, including the separated region, little improvement is gained using the v2f model and in general the turbulent kinetic energy prediction is fair at best.

Intentionally Left Blank

Acknowledgments

Special thanks to Greg Evans, Chris Moen and Stefan Domino for assistance on a variety of issues concerning SIERRA/Fuego and the compute clusters.

Contents

FIGURES

TABLES

Introduction

The effect of curvature on fluid turbulence has long since been of interest to the geophysical and astrophysical fluid dynamics communities as well as numerous engineering disciplines. The original motivation for studying flow through a serpentine passage stemmed from a desire to better predict the turbulent flowfield in the internal cooling passages found in airplane turbine blades (Laskowski, 2004). Since gas turbine engine performance is a strong function of the turbine inlet temperature, and in order to ensure that the structural integrity of turbine blades is not compromised at high temperatures, elaborate cooling strategies are often required. One such approach is to siphon relatively low temperature fluid from the compressor and circulate it through the turbine blade internal serpentine passages. These passages are often ribbed to enhance turbulent mixing and facilitate enhanced heat transfer. The fluid is then injected into the external flow through small holes near the blade leading edge and slots near the trailing edge for film cooling purposes (Medic and Durbin, 2002). A fundamental understanding of the turbine blade external turbulent flow (Laskowski et al., 2004) as well as the internal turbulent flow is required to improve heat transfer predictions. The design of effective and efficient turbine blade thermal management systems is strongly rooted in the ability to predict the heat transfer which requires a fundamental representation of the turbulent flow-field that exists in the internal passage. This is no easy task and the design can be quite challenging due to strong curvature, ribs, thermal buoyancy and strong rotational effects. While Reynolds Average Navier Stokes (RANS) modeling approaches can be used in the design cycle of the thermal management system, and can account for varying degrees of geometric complexity (Iacarrino et al., 2003), the design and calibration of turbulence models requires detailed information that can be supplied by Direct Numerical Simulations (DNS) and/or physical experiments.

Numerous experiments investigating the turbulent flow-field in stationary U-bends have been conducted [Sandborn and Shin (1989); Monson et al. (1990); Cheah et al. (1994); Okita et al. (2003)] and corresponding RANS computational results for eddy viscosity models (EVM), algebraic stress models (ASM) and full second moment closure models (SMC) have been documented [Li (1995); Iacovides et al. (1996); Luo and Lakshminarayana (1997); Parneix et al. (1998); Rumsey et al. (1999); Iacovides et al. (2000); Shur et al. (2000); Chen and Han (2002); Okita and Iacovides (2003)]. While curvature corrected eddy viscosity models have met with some success (Shur et al., 2000), it is generally recognized that ASM or SMC models are required to capture the strong anisotropy that exists in such flows. The level of success that different models can be expected to achieve is dependent on databases available for calibration and comparison.

One shortcoming of experimental measurements of such flows is lack of resolution, especially near solid surfaces. Furthermore, certain statistical moments of interest, including pressure strain and dissipation, can prove exceedingly difficult to obtain, yet are of interest to the turbulence modeling community. Laskowski (2004) conducted a DNS study to investigate the coupled effect of strong curvature and rotation by simulating turbulent flow through a fully developed, smooth wall, round-ended, isothermal serpentine passage subjected to orthogonal mode rotation. The geometry investigated had dimensions $12\pi\delta$ x 2δ x $3\pi\delta$ in the stream-wise, transverse and span-wise directions and has a radius of curvature $\delta/r_c = 0.5$ in the curved section. The computational domain consisted of pseudo-periodic inflow-outflow boundaries, two solid wall boundaries, and periodic boundaries in the span-wise direction. Periodic boundary conditions were utilized in the homogeneous span-wise direction to accelerate convergence of the statistics and to reduce the instantaneous 3D time dependent problem to a 2D statistical steady state problem. DNS simulations were carried out for $Re_b = 5500$ and $\delta/R = 0.5$. The idealized geometry models turbine blade internal cooling passages and provides an attractive database to validate turbulence models responsiveness to flows subjected to strong curvature and rotation.

Since linear eddy-viscosity turbulence models have become the workhorse of commercial and research codes for the solution of complex engineering fluid dynamic's problems, it is imperative to document the degree of accuracy that can be expected from the models for relatively simple problems which contain similar physics. This is particularly true for flows where certain turbulence model assumptions may violate the actual physics. For example, it is well documented that these types of models can yield erroneous results for certain classes of problems which include strong curvature, rotation, thermal buoyancy and three-dimensional boundary layers (Durbin and Reif, 2001). Unfortunately, increasingly complex turbulence models which include non-linear eddy viscosity models, explicit and implicit algebraic stress models and full second moment closure models, can prove to be very difficult to converge if not prohibitively expensive for complex flows. A tradeoff exists between accuracy, stability and efficiency. While it is certainly acceptable to use linear eddy viscosity models in flow regimes where they were not initially intended, it is important to be able to ascertain the level of error that can be expected for certain quantities of interest such as mean velocity field, turbulent kinetic energy field, turbulent time scale field and so forth. The stationary DNS results of Laskowski (2004) were selected as an attractive test case for a Fuego v2f model V&V and the purpose of this report is to document Fuego's v2f model results compared to DNS and results obtained with the very common two-layer k-ε model.

Turbulence Simulation and Modeling

The Navier-Stokes equations, with appropriate boundary and initial conditions, completely describe fluid flow, including turbulence. Incompressible fluid flow will be assumed for illustrative purposes. Eq. (1) presents the Navier-Stokes equations in differential form for an incompressible flow with a thermal buoyancy force utilizing the Boussinesq approximation:

$$\begin{aligned}
&\frac{\partial(U_j)}{\partial x_j} = 0 \\
&\frac{\partial(U_i)}{\partial t} + \frac{\partial(U_i U_j)}{\partial x_j} = -\frac{1}{\rho}\frac{\partial P}{\partial x_i} + \nu\frac{\partial}{\partial x_j}\left(\frac{\partial U_i}{\partial x_j}\right) - g_i\beta(\Theta - \Theta_r) \\
&\frac{\partial(\Theta)}{\partial t} + \frac{\partial(U_j\Theta)}{\partial x_j} = \frac{\mu}{\rho \mathrm{Pr}}\frac{\partial}{\partial x_j}\left(\frac{\partial \Theta}{\partial x_j}\right)
\end{aligned} \tag{1}$$

The exact solution of Eq. (1) using accurate numerical schemes for all length and time scales is referred to as DNS, or Direct Numerical Simulation. The grid and time step requirements for DNS simulations scale nonlinearly with Reynolds number (Wilcox, 2000). For real world engineering type applications, DNS is currently unrealistic. Rather, DNS is a useful tool to assist in the development of models to account for the effect of turbulence for simulations to be run on much coarser grids and at much larger time steps.

An alternative to simulating turbulence via the exact solution of Eq. (1) is to model it. In order to do so the dependent variables in Eq. (1) are replaced with:

$$\begin{aligned}
U_j &= \overline{U_j} + u_j' \\
P &= \overline{P} + p' \\
\Theta &= \overline{\Theta} + \theta'
\end{aligned} \tag{2}$$

which is to say that the instantaneous value is represented as the sum of a time averaged value and a perturbation. Upon substitution, Eq. (1) is then averaged in time:

$$\overline{\frac{\partial\left(\overline{U_j}+u_j'\right)}{\partial x_j}=0}$$

$$\overline{\frac{\partial\left(\overline{U_i}+u_i'\right)}{\partial t}+\frac{\partial\left(\left(\overline{U_i}+u_i'\right)\left(\overline{U_j}+u_j'\right)\right)}{\partial x_j}=-\frac{1}{\rho}\frac{\partial\left(\overline{P}+p'\right)}{\partial x_i}+\nu\frac{\partial}{\partial x_j}\left(\frac{\partial\left(\overline{U_i}+u_i'\right)}{\partial x_j}\right)-g_i\beta\left(\overline{\Theta}+\theta'-\Theta_r\right)} \quad (3)$$

$$\overline{\frac{\partial\left(\overline{\Theta}+\theta'\right)}{\partial t}+\frac{\partial\left(\left(\overline{U_j}+u_j'\right)\left(\overline{\Theta}+\theta'\right)\right)}{\partial x_j}=\frac{\mu}{\rho \mathrm{Pr}}\frac{\partial}{\partial x_j}\left(\frac{\partial\left(\overline{\Theta}+\theta'\right)}{\partial x_j}\right)}$$

Taking the time average of Eq. (3), using the identity $\overline{\partial\left(\phi'\right)/\partial x_j}=0$ and subtracting this from Eq. (1) results in the Reynolds Averaged Navier Stokes (RANS) equations:

$$\frac{\partial\left(\overline{U_j}\right)}{\partial x_j}=0$$

$$\frac{\partial\left(\overline{U_i}\right)}{\partial t}+\frac{\partial\left(\overline{U_i}\,\overline{U_j}\right)}{\partial x_j}=-\frac{1}{\rho}\frac{\partial\overline{P}}{\partial x_i}+\nu\frac{\partial}{\partial x_j}\left(\frac{\partial\overline{U_i}}{\partial x_j}-\overline{u_i'u_j'}\right)-g_i\beta\left(\overline{\Theta}-\Theta_r\right) \quad (4)$$

$$\frac{\partial\left(\overline{\Theta}\right)}{\partial t}+\frac{\partial\left(\overline{U_j}\,\overline{\Theta}\right)}{\partial x_j}=\frac{\mu}{\rho \mathrm{Pr}}\frac{\partial}{\partial x_j}\left(\frac{\partial\overline{\Theta}}{\partial x_j}-\overline{u_j'\theta'}\right)$$

It is evident that the nonlinear nature of the advection term in Eq. (1) has resulted in an additional term in the time averaged sense which must be modeled. The additional terms in Eq. (4) are referred to as the Reynolds stresses and turbulent fluxes. Numerous simplifying assumptions were used to arrive at Eq. (4), namely: assumption of constant density (ρ), assumption of constant viscosity (μ) and assumption of constant coefficient of thermal expansion (β). In reality all three are temperature dependent and vary both spatially and temporally.

A transport equation for the Reynolds stresses can be obtained by performing the time average:

$$\overline{u_j'\left[\frac{\partial\left(U_i\right)}{\partial t}+\frac{\partial\left(U_iU_j\right)}{\partial x_j}+\frac{1}{\rho}\frac{\partial P}{\partial x_i}-\nu\frac{\partial}{\partial x_j}\left(\frac{\partial U_i}{\partial x_j}\right)+g_i\beta\left(\Theta-\Theta_r\right)\right]+u_i'\left[\frac{\partial\left(U_j\right)}{\partial t}+\frac{\partial\left(U_jU_i\right)}{\partial x_j}+\frac{1}{\rho}\frac{\partial P}{\partial x_i}-\nu\frac{\partial}{\partial x_j}\left(\frac{\partial U_j}{\partial x_j}\right)+g_j\beta\left(\Theta-\Theta_r\right)\right]=0} \quad (5)$$

$$\overline{u_i'\left[\frac{\partial\left(\Theta\right)}{\partial t}+\frac{\partial\left(U_j\Theta\right)}{\partial x_j}-\frac{\mu}{\rho \mathrm{Pr}}\frac{\partial}{\partial x_j}\left(\frac{\partial\Theta}{\partial x_j}\right)\right]+\theta'\left[\frac{\partial\left(U_i\right)}{\partial t}+\frac{\partial\left(U_iU_j\right)}{\partial x_j}+\frac{1}{\rho}\frac{\partial P}{\partial x_i}-\nu\frac{\partial}{\partial x_j}\left(\frac{\partial U_i}{\partial x_j}\right)+g_i\beta\left(\Theta-\Theta_r\right)\right]=0}$$

where again the dependent variables in Eq. (5) are defined by Eq. (2). After considerable algebra, the transport equations resulting from the momentum and energy equations can now be written:

$$\underbrace{\frac{D\overline{u_i'u_j'}}{Dt}}_{\text{Convection}} - \underbrace{\frac{\partial}{\partial x_k}\left(\nu\frac{\partial\overline{u_i'u_j'}}{\partial x_k}\right)}_{\text{Viscous diffusion}} = \underbrace{P_{ij}}_{\text{Production due to shear}} + \underbrace{G_{ij}}_{\text{Production due to buoyancy}} + \underbrace{\varepsilon_{ij}}_{\text{Dissipation}} - \underbrace{\Pi_{ij}}_{\text{Pressure strain}} + \underbrace{D_{ij}}_{\text{Turbulent diffusion}}$$

$$\frac{D\overline{u_i'\theta'}}{Dt} - \frac{\partial}{\partial x_k}\left(\nu\overline{\theta'\frac{\partial u_i'\theta'}{\partial x_k}} + a\overline{u_i'\frac{\partial\theta'}{\partial x_k}}\right) = P_{\theta i} + G_{\theta i} + \varepsilon_{\theta i} - \Pi_{\theta i} + D_{\theta i} \tag{6}$$

Numerous approaches have been used to model the Reynolds stresses, the most common of which are the so called "Eddy Viscosity" models which assume isotropy and are based in large part on the Boussinesq hypothesis:

$$-\overline{u_i'u_j'} \equiv \tau_{ij}^{turb}/\rho = 2\nu_T S_{ij} - \frac{2}{3}k\delta_{ij}$$

where (7)

$$S_{ij} = \frac{1}{2}\left(\frac{\partial\overline{U_i}}{\partial x_j} + \frac{\partial\overline{U_j}}{\partial x_i}\right)$$

in order to redefine the momentum equation as:

$$\frac{\partial\left(\overline{U_i}\right)}{\partial t} + \frac{\partial\left(\overline{U_i}\,\overline{U_j}\right)}{\partial x_j} = -\frac{1}{\rho}\frac{\partial\overline{P}}{\partial x_i} + \frac{\partial}{\partial x_j}\left[\left(\nu+\nu_T\right)\left(\frac{\partial\overline{U_i}}{\partial x_j}\right)\right] - g_i\beta\left(\overline{\Theta} - \Theta_r\right) \tag{8}$$

The energy equation typically receives less attention, and for forced convection problems the turbulent heat flux is a function of the eddy viscosity and temperature gradient:

$$-\overline{u_j'\theta'} = \frac{\nu_T}{Pr_T}\frac{\partial\bar{\theta}}{\partial x_j} \tag{9}$$

where Pr_T is the turbulent Prandtl number which is assumed to be constant and equal to 0.91. For flows in the mixed or free convection regime, more details regarding the closure of the energy equation may be needed (Kenjeres, 1999).

The most common way of determining the eddy viscosity in Eq. (7) is via the solution of 1, 2 or more transport equations for certain scalar turbulence quantities. By far the most common approach follows from Jones and Launder's (1972) k-ε model. The turbulent kinetic energy, $k = \overline{u_i' u_i'}/2$, can be determined by taking the trace of the momentum Reynolds stress transport equation resulting in:

$$\underbrace{\frac{Dk}{Dt}}_{\substack{\text{Convection}\\ \text{of}\\ \text{turbulent}\\ \text{kinetic}\\ \text{energy}}} = \underbrace{P}_{\substack{\text{Production}\\ \text{of}\\ \text{turbulent}\\ \text{kinetic}\\ \text{energy}}} - \underbrace{\varepsilon}_{\substack{\text{Dissipation}\\ \text{of}\\ \text{turbulent}\\ \text{kinetic}\\ \text{energy}}} + \underbrace{\frac{\partial}{\partial x_k}\left(\left(\nu + \frac{\nu_T}{\sigma_k}\right)\frac{\partial k}{\partial x_k}\right)}_{\substack{\text{Diffusion}\\ \text{of}\\ \text{turbulent}\\ \text{kinetic}\\ \text{energy}}} \tag{10}$$

where P is the scalar production, $P = \tau_{ij}^{turb}\, \partial \overline{U}_i / \partial x_j$ and ε is the scalar dissipation which is solved for via another transport equation the structure of which mimics the k transport equation:

$$\underbrace{\frac{D\varepsilon}{Dt}}_{\substack{\text{Convection}\\ \text{of}\\ \text{dissipation}}} = \underbrace{C_{\varepsilon 1}\frac{\varepsilon}{k}P}_{\substack{\text{Production}\\ \text{of}\\ \text{dissipation}}} - \underbrace{C_{\varepsilon 2}\frac{\varepsilon^2}{k}}_{\substack{\text{Dissipation}\\ \text{of}\\ \text{dissipation}}} + \underbrace{\frac{\partial}{\partial x_k}\left(\left(\nu + \frac{\nu_T}{\sigma_\varepsilon}\right)\frac{\partial \varepsilon}{\partial x_k}\right)}_{\substack{\text{Diffusion}\\ \text{of}\\ \text{dissipation}}} \tag{11}$$

and the turbulent viscosity is constructed based on the computed values of k-ε:

$$\nu_T = C_\mu \frac{k^2}{\varepsilon} \tag{12}$$

where $C_\mu = 0.09$ is based on the assumption of production/dissipation equilibrium in the log-layer and experimental observations of the ratio of Reynolds stress to turbulent kinetic energy (Durbin and Reif, 2001).

Near Wall Effects

Equations (10-11) were developed primarily for free shear flows and boundary layers. Additional modeling is required in flows where solid walls are present (refer to Laskowski (1999) for additional details). The predictions for two models will be presented, namely the two layer k-ε model (Chen and Patel, 1988) and the v2f model of Durbin (1991).

Two Layer k-ε Model

One common approach regarding the near wall treatment of turbulence in two equation models is the 2-layer method where Eqs. (10-11) are solved in the "Outer Layer" and Eq. (10) is solved in the "Inner Layer" with a length scale (dissipation) that is determined algebraically:

$$\nu_T = C_\mu \sqrt{k} l_\nu$$
$$l_\nu = C_l y\left(1 - e^{-Re_y/A_\nu}\right), \quad C_l = \kappa C_\mu^{-3/4}; \quad A_\nu = 2C_l; \quad Re_y = \frac{\rho y \sqrt{k}}{\mu} \tag{13}$$

where $\kappa = 0.41$ is the von Karman constant. The switch to the inner layer is determined when:

$$\left(1 - e^{-Re_y/A_\nu}\right) \leq 0.95 \tag{14}$$

The model closure coefficients are presented in Table 1.

Table 1. Closure coefficients for two layer k-ε model.

C_μ	$C_{\varepsilon 1}$	$C_{\varepsilon 2}$	σ_k	σ_ε
0.09	1.44	1.92	1.0	1.3

Original v2f Model

An alternative to using damping functions was detailed by Durbin (1991) who developed the v2f model which utilizes elliptic relaxation, includes more details in terms of the pressure-strain redistribution, retains a certain degree of near-wall anisotropy, and includes lower bounds on length and time scales to account for improved near wall effects. Refer to Durbin (2001) for more details

concerning the model. The k equation is identical to Eq. (10) and slight modifications to the turbulent time scale are made to the dissipation equation, Eq. (11):

$$\frac{D\varepsilon}{Dt} = C_{\varepsilon 1}^{*}\frac{1}{T}P - C_{\varepsilon 2}^{*}\frac{1}{T}\varepsilon + \frac{\partial}{\partial x_k}\left(\left(\nu + \frac{\nu_T}{\sigma_\varepsilon^{*}}\right)\frac{\partial \varepsilon}{\partial x_k}\right) \tag{15}$$

Two new transport equations for the wall normal variance and variance redistribution, which stems from modeling approaches for Second Moment Closure (SMC) pressure-strain modeling, are introduced. The new transport equations for $v2$ and f are:

$$\begin{aligned} \frac{D\overline{v'^2}}{Dt} &= kf - n\overline{v'^2}\frac{\varepsilon}{k} + \frac{\partial}{\partial x_k}\left(\left(\nu + \frac{\nu_T}{\sigma_{v2}^{*}}\right)\frac{\partial \overline{v'^2}}{\partial x_k}\right) \\ L^2\nabla^2 f - f &= \frac{1}{T}\left[(C_1 - n)\frac{\overline{v'^2}}{k} - (C_1 - 1) - \frac{2}{3}\right] - C_2\frac{P}{k} \end{aligned} \tag{16}$$

where turbulent time scale, T, is defined as:

$$\begin{aligned} T &= \min\left[\max\left[\frac{k}{\varepsilon}, 6\sqrt{\frac{\nu}{\varepsilon}}\right], \frac{0.6k}{\sqrt{6}C_\mu \overline{v'^2} S}\right] \\ S &= \left(S_{ij}S_{ij}\right)^{1/2} \\ S_{ij} &= \frac{1}{2}\left(\frac{\partial \overline{U_i}}{\partial x_j} + \frac{\partial \overline{U_j}}{\partial x_i}\right) \end{aligned} \tag{17}$$

and turbulent length scale, L, is defined as:

$$L = C_L \max\left(\min\left(\frac{k^{3/2}}{\varepsilon}, \frac{k^{3/2}}{2\sqrt{3}C_\mu \overline{v^2} S}\right), C_\eta \frac{\nu^{3/4}}{\varepsilon^{1/4}}\right) \tag{18}$$

Finally, the turbulent viscosity is computed based on the computed values of *v2* and *T*:

$$\nu_T = C_\mu \overline{v'^2} T \tag{19}$$

The model closure coefficients for the v2f model are listed in Table 2.

Table 2. Original v2f closure coefficients.

C_μ	$C^*_{\varepsilon 1}$	$C^*_{\varepsilon 2}$	C_1	C_2	σ^*_k	σ^*_ε	σ^*_{v2}	n	C_L	C_η	A_ε
0.22	$C_{\varepsilon 1}\left(1+0.045\sqrt{k/\overline{v^2}}\right)$	1.92	1.4	0.3	1.0	1.3	1.0	6	0.23	70	0.00285

Intentionally Left Blank

Modified v2f Model

Numerous stability issues have been encountered in Fuego with the original formulation of the v2f model for low Re number flows (Evans, 2004). An approach similar to that proposed by Sveningsson (2003) on the treatment of the turbulent time scale yielded a more stable model. However, in his thesis Sveningsson note's that "*The obvious solution to this anomaly is to not use the realizability constraint in the f equation or to change the modeled v2 dissipation rate. One of these modifications proved to be necessary in order to achieve a converged solution for the stator vane computations...*". Note that he advocates using one of the fixes, not both as is currently being done. Additionally, the realizability constraint is omitted from the turbulence length scale in the Fuego modified formulation. Table 3 presents the original v2f model and the modified "stabilized" v2f model currently in Fuego[1] and Table 4 presents the closure coefficients for this model.

Table 3. Modified v2f model variations.

	Fuego modified formulation	Original formulation
T: f-eqn.	$T = TT1 = \max\left[\frac{k}{\varepsilon}, C_T\left(\frac{\nu}{\varepsilon}\right)^{1/2}\right]$	$T = TT = \min\left\{\max\left[\frac{k}{\varepsilon}, C_T\left(\frac{\nu}{\varepsilon}\right)^{1/2}\right], \frac{\alpha k}{\sqrt{6}\overline{v^2}C_\mu\lvert S\rvert}\right\}$
T: v2 eqn	$T = TT1 = \max\left[\frac{k}{\varepsilon}, C_T\left(\frac{\nu}{\varepsilon}\right)^{1/2}\right]$	$T = TT2 = \frac{k}{\varepsilon}$
T: eps eqn	$T = TT = \min\left\{\max\left[\frac{k}{\varepsilon}, C_T\left(\frac{\nu}{\varepsilon}\right)^{1/2}\right], \frac{\alpha k}{2\sqrt{3}\overline{v^2}C_\mu\lvert S\rvert}\right\}$	$T = TT = \min\left\{\max\left[\frac{k}{\varepsilon}, C_T\left(\frac{\nu}{\varepsilon}\right)^{1/2}\right], \frac{\alpha k}{\sqrt{6}\overline{v^2}C_\mu\lvert S\rvert}\right\}$
T: mut-eqn	$T = TT = \min\left\{\max\left[\frac{k}{\varepsilon}, C_T\left(\frac{\nu}{\varepsilon}\right)^{1/2}\right], \frac{\alpha k}{2\sqrt{3}\overline{v^2}C_\mu\lvert S\rvert}\right\}$	$T = TT = \min\left\{\max\left[\frac{k}{\varepsilon}, C_T\left(\frac{\nu}{\varepsilon}\right)^{1/2}\right], \frac{\alpha k}{\sqrt{6}\overline{v^2}C_\mu\lvert S\rvert}\right\}$
L: f-eqn.	$L = C_L \max\left(\frac{k^{3/2}}{\varepsilon}, C_\eta \frac{\nu^{3/4}}{\varepsilon^{1/4}}\right)$	$L = C_L \max\left\{\min\left(\frac{k^{3/2}}{\varepsilon}, \frac{k^{3/2}}{\sqrt{6}C_\mu \overline{v^2}S}\right), C_\eta \frac{\nu^{3/4}}{\varepsilon^{1/4}}\right\}$

[1] Note: The value 2sqrt(3) in the denominator of the turbulent time scale of the "Fuego modified formulation" is incorrect and should be corrected to sqrt(6).

Table 4. Modified v2f closure coefficients.

C_μ	$C_{\varepsilon 1}^*$	$C_{\varepsilon 2}^*$	C_1	C_2	σ_k^*	σ_ε^*	σ_{v2}^*	n	C_L	C_η	A_ε
0.22	$C_{\varepsilon 1}\left(1+0.045\sqrt{k/\overline{v^2}}\right)$	1.92	1.4	0.3	1.0	1.0	1.0	6	0.23	70	0.00285

Codes and Models

Laskowski (2004) conducted DNS simulations of flow through a serpentine passage both with and without orthogonal mode rotation to study the coupled effect of rotation and curvature. The incompressible Navier-Stokes equations were solved with a refactored version of the DNS code originally developed by Wu and Durbin (2001) which is based on the finite volume projection algorithm of Rosenfeld et al. (1991). The dependent variables are the volume fluxes across each face of the computational cells. Spatial derivatives are discretized with 2^{nd} order central differences. The convection term is advanced via 2^{nd} order Adams-Bashforth time integration and the diffusion term is advanced using the 2^{nd} order Crank-Nicholson. The pressure Poisson equation is solved using V-cycle multigrid in the x-y plane and a Fast Fourier Transform (FFT) in the spanwise direction. Extensive numerical tests were conducted which included turbulent channel flow simulations, rotating channel flow simulations, and grid and domain independence tests. The results will be used to investigate the performance of RANS eddy-viscosity models subjected to strong curvature. Rotational effects will not be considered as Fuego (2002) does not support rotation at the present time.

Results are presented for STAR-CD (1999), a commercial software package; Fuego[2] (Moen et al., 2002), an unstructured low Mach number code for the simulation of large pool fires; CORANS a 3D compressible, structured, block-implicit conservative code developed by Laskowski (2004) based on the algorithm of MacCormack and Pulliam (1998). The codes/models are summarized in Table 5.

[2] Appendix A contains the input file used for the FUEGO simulations.

Table 5. Codes and models for serpentine passage V&V study.

	CODE	CODE REGIME	CODE TYPE	EAST/WEST BOUNDARY CONDITION	TURB. MODEL	TURB. MODEL TYPE
CASE 1	DNS	Incompressible	DNS	Profile Inflow & Convection Outflow ~ Periodic	None-Turbulence Simulated	N/A
CASE 2	Fuego	Low Mach Number	RANS	Plug Inflow & Open Outflow	V2f	Linear Eddy Viscosity
CASE 3	CORANS	Compressible	RANS	Plug Inflow & Convection Outflow	2 Layer k-ε	Linear Eddy Viscosity
CASE 4	STAR-CD	Commercial (Incompressible & Compressible)	RANS	True Periodic	2 Layer k-ε	Linear Eddy Viscosity

Results

Whereas 3D time dependent simulation were conducted in Case 1, Cases 2-4 were conducted on 2D meshes, for the same grid resolution, at large time steps in order to arrive at a statistical steady state. Figure 1 presents the 2D geometry and the various station locations of interest. Results are presented in non-dimensional form based on the average friction velocity:

$$U = \frac{u}{u_\tau}; \quad K = \frac{k}{u_\tau^2}$$
$$u_\tau = \frac{1}{S}\int_{S_0}^{S_L} u_\tau(s)\,ds; \quad u_\tau(s) = \sqrt{\frac{\tau_w}{\rho}} \tag{19}$$

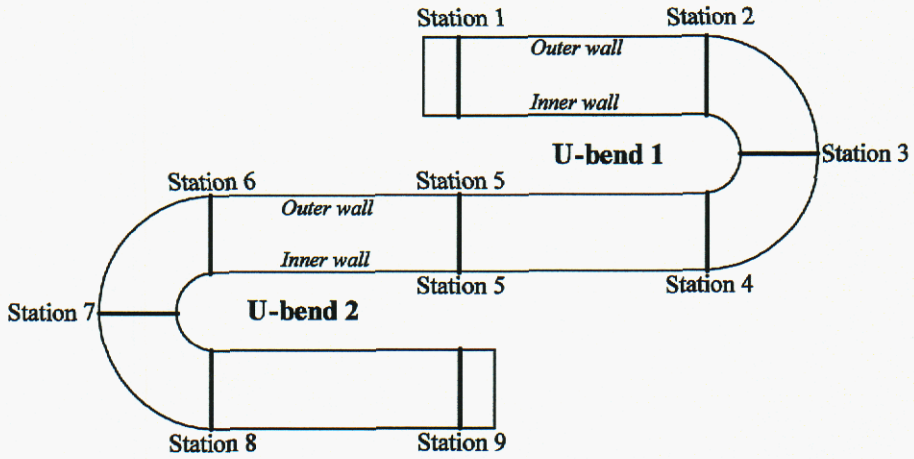

Figure 1. 2D geometry and station locations.

The DNS simulations utilized periodic east/west (inflow/outflow) boundary conditions. This particular boundary condition is not available in Fuego nor is it available in CORANS. As a work around, three full periods of the serpentine passage simulation were simulated and a plug flow was specified at inflow and convective outflow condition specified at outflow. The DNS simulation results were used as a guide for the specification of the inflow boundary conditions. As the flow enters the third serpentine the flow results are insensitive to the prescribed inflow boundary

conditions. Figure 2 presents the static pressure for Cases 2-4. The sensitivity to the inflow values of turbulence was found to be quite negligible as the flow became fully developed and is depicted in Figure 3.

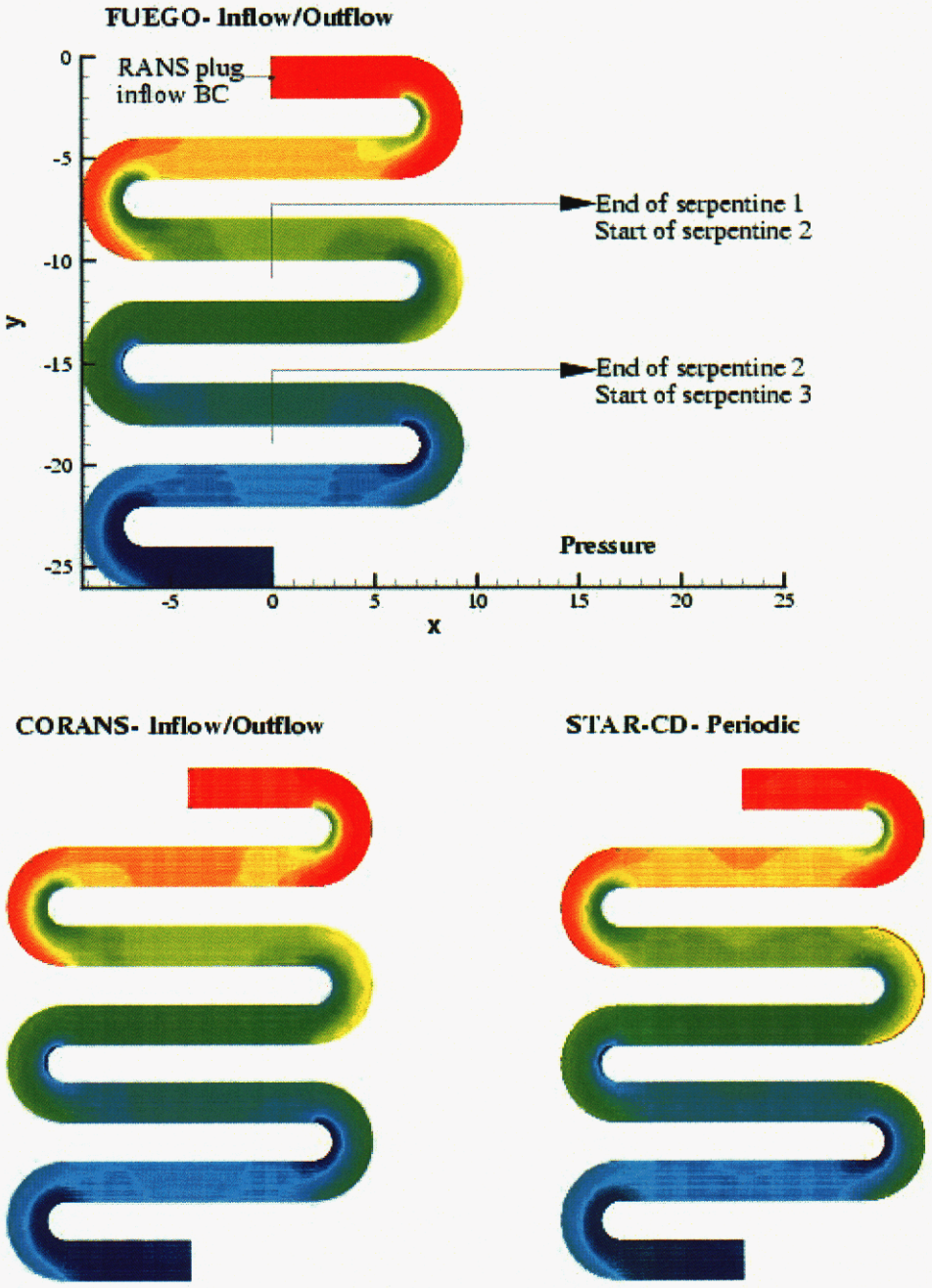

Figure 2. Comparison of static pressure for Case 2, Case 3 and Case 4.

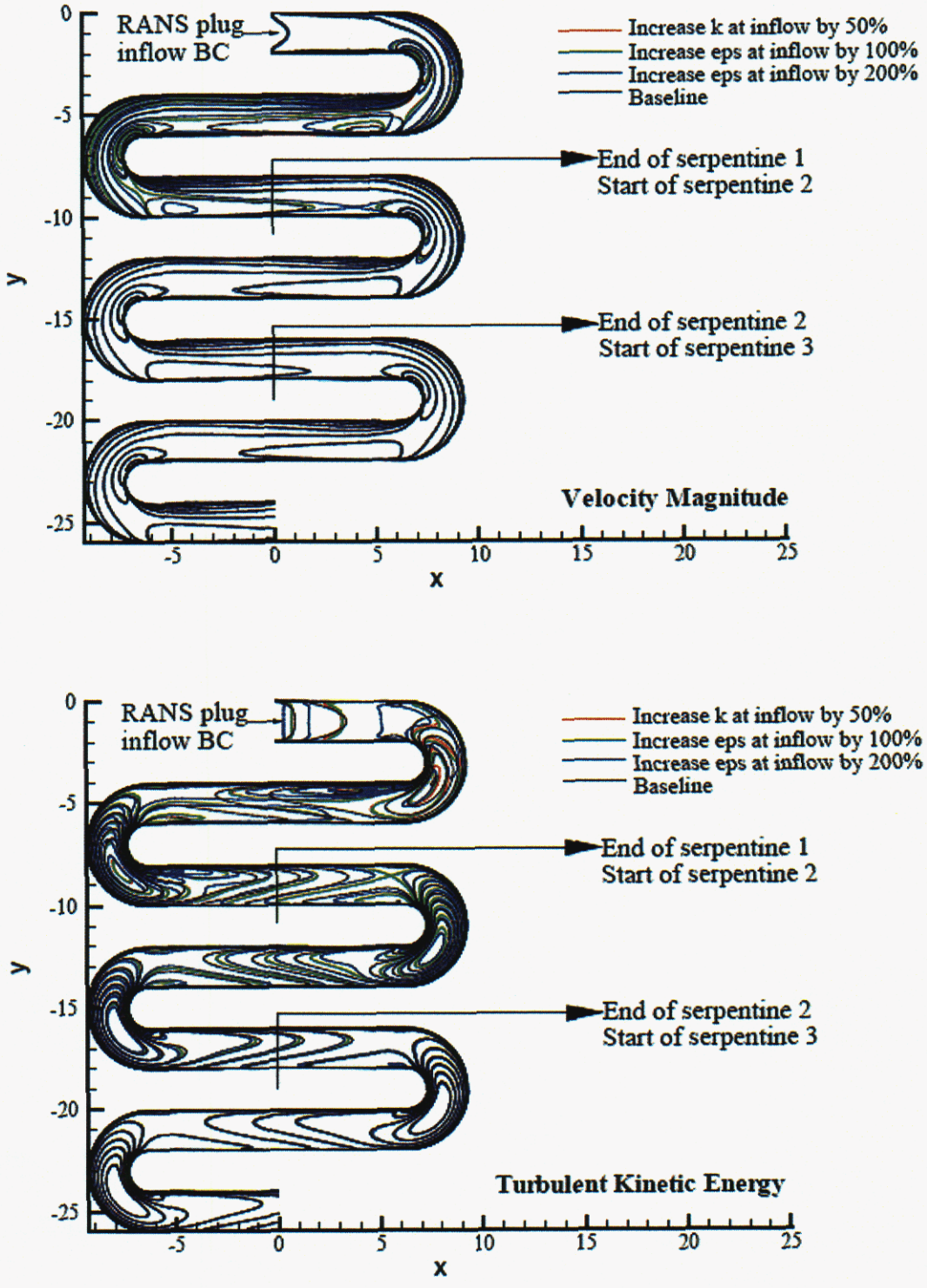

Figure 3. Sensitivity to inflow turbulence for RANS simulations (Case 2).

Figure 4 presents residual behavior for Case 2 (Fuego, Original v2f) and Case 3 (CORANS, k-ε) demonstrating the drive to steady state. All residuals are normalized based on their initial value to demonstrate order of magnitude convergence. Concerning Case 1, excellent residual behavior is demonstrated for all equations. The residual behavior for Case 2 is excellent as well, however the level of convergence is less than what is observed in Case 1. The lower levels of convergence observed in Case 3 can be attributed to the fact that CORANS is a fully implicit compressible code which solves the equations in a coupled manner. Density variations were on the order of 1% and the code does not allow for preconditioning. Correspondingly, the eigenvalues of the flux Jacobians become very small and the system is not well conditioned.

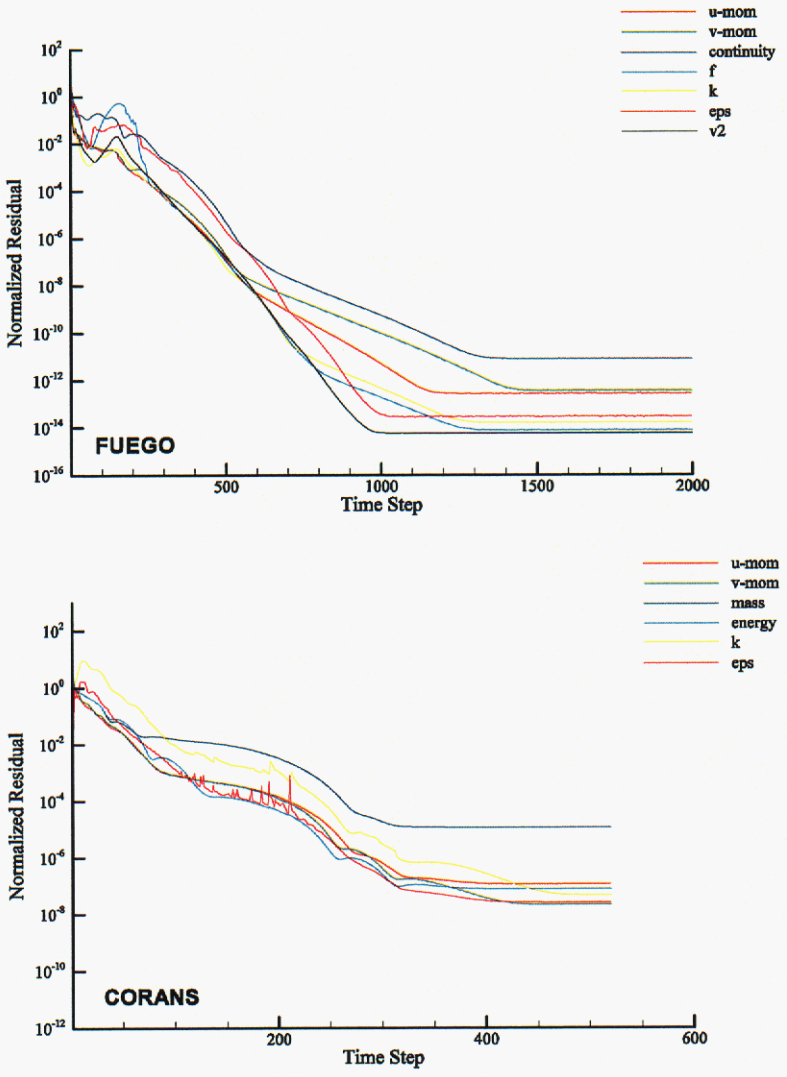

Figure 4. Residual behavior for Fuego and CORANS.

Figures (5-7) present the Cartesian u,v,w velocity components for Case 1 and 2 in the xy plane. The true turbulent nature of the flow from the DNS results can be observed in Figure 5a, 6a and 7a which depicts the instantaneous values of Cartesian u,v,w at some arbitrary instant in time. Again, the DNS code is solving Eq. (1) (less the temperature equation) on a 3D, highly refined mesh using 2^{nd} order time integration and 2^{nd} order spatial representation of the flow, resolving all time and length scales down to on order of the Kolmogorov scale. The time averaged DNS result are presented in Figures 5b, 6b and 7b while the steady state results for Case 2 are presented in Figures 5c, 6c, 7c. In Case 2 the governing equations in Eq. (4) are being solved and the turbulence parameter ν_T is modeled via the original v2f model described earlier. The aim of the RANS model is to arrive at the time average of the flow plotted in Figure 5b, 6b, 7b thus bypassing the time dependant, three dimensional nature of the problem. This can be understood by looking at the converged residuals of Fig. 4 for Case 2, $\partial(\ )/\partial t = 0$ after 1000 time steps.

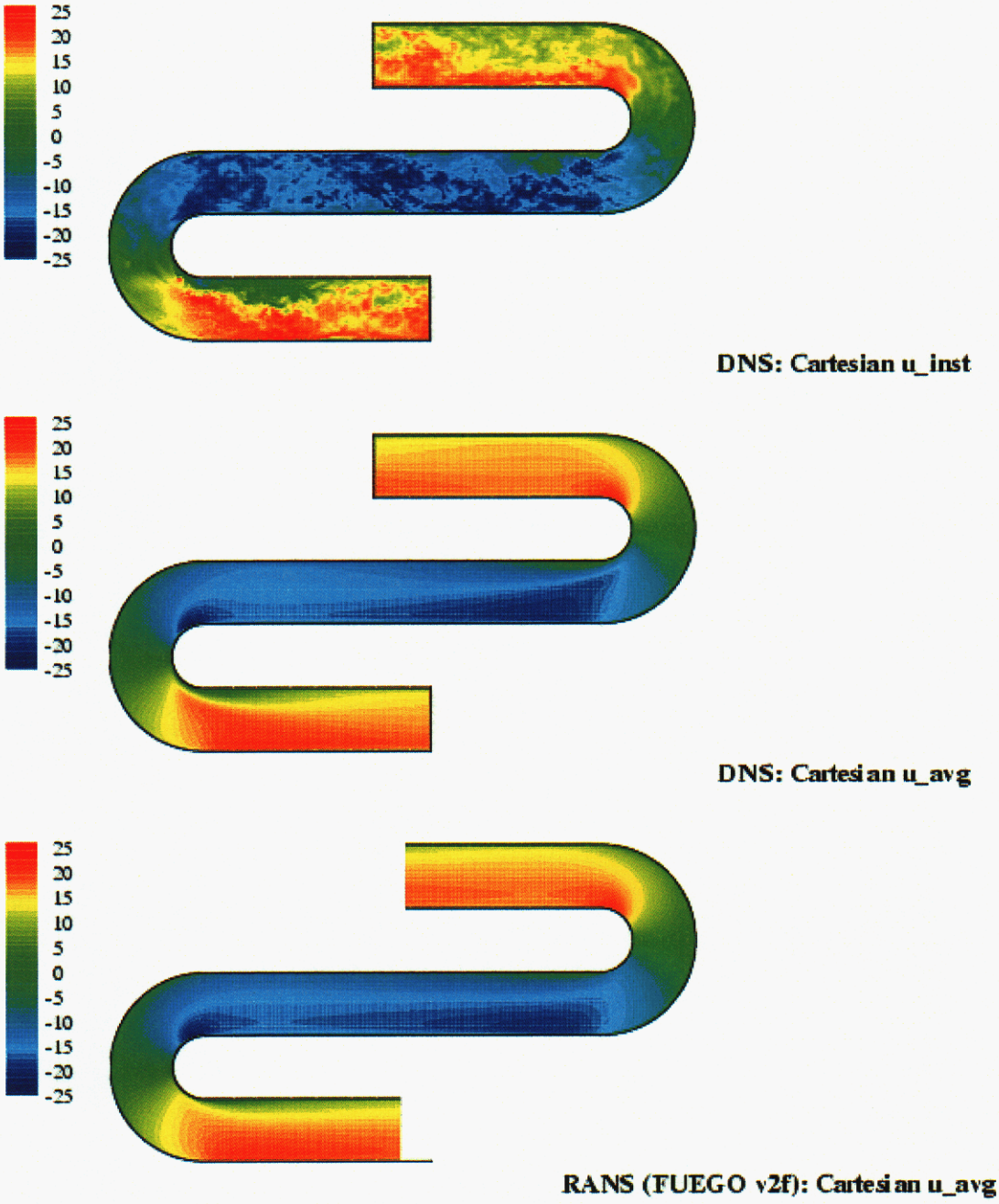

Figure 5. Comparison of Cartesian u component of velocity (Case 1 and Case 2).

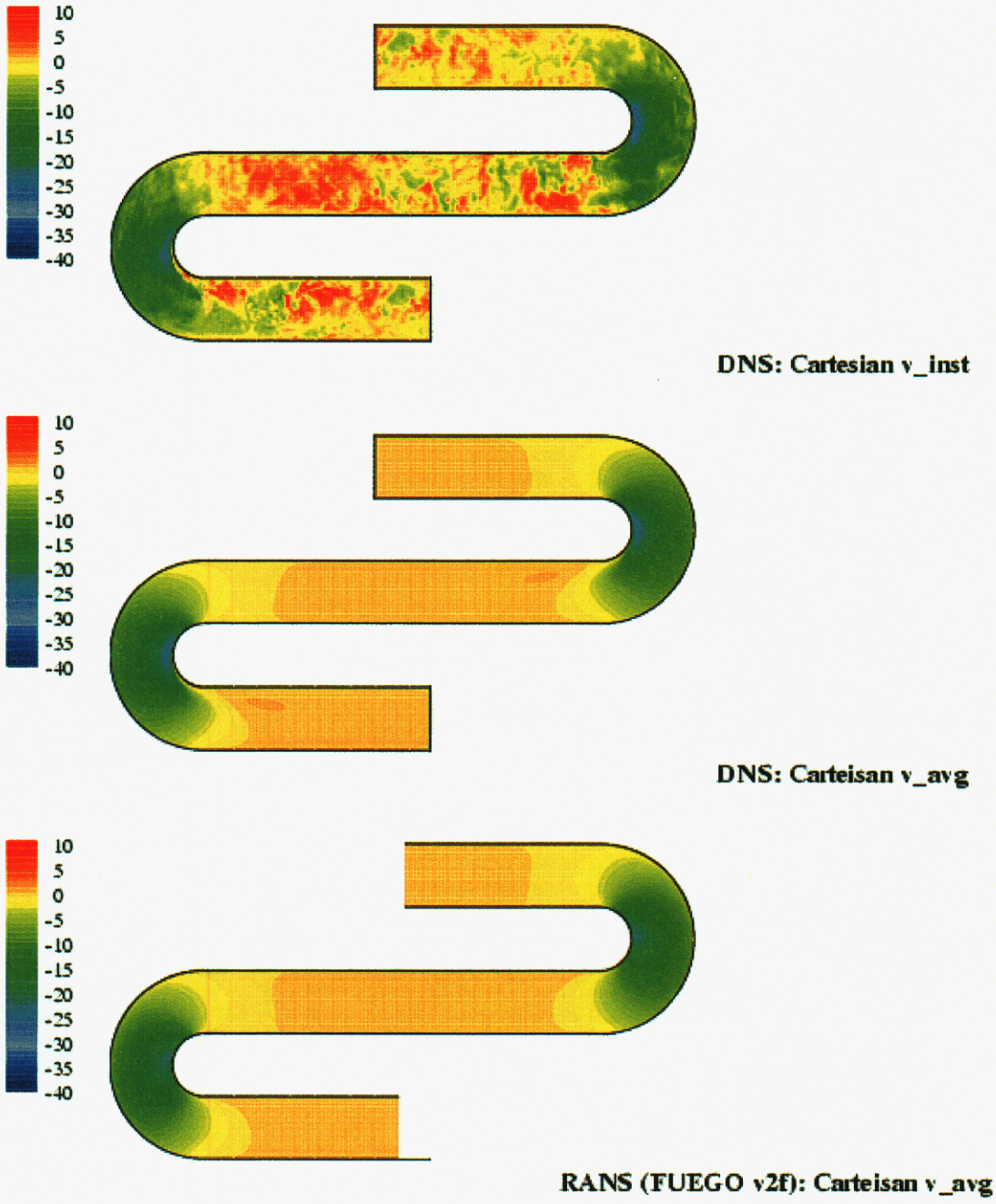

Figure 6. Comparison of Cartesian v component of velocity (Case 1 and Case 2).

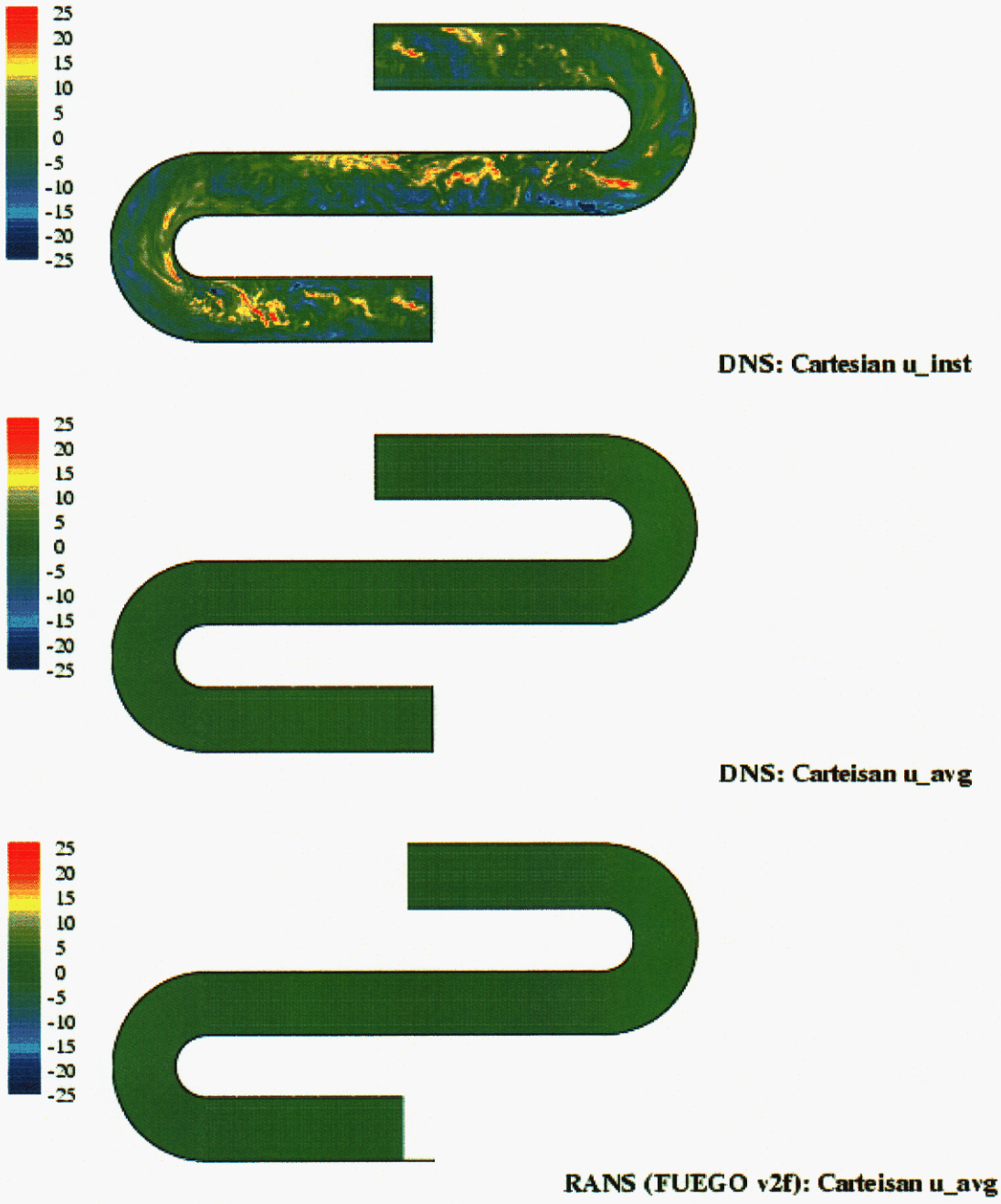

Figure 7. Comparison of Cartesian w component of velocity (Case 1 and Case 2).

In order to better depict the level of agreement between Cases 2-4 and Case 1, contours for the averaged Cartesian u and v components, velocity magnitude and turbulent kinetic energy are presented in Figures 8-11.

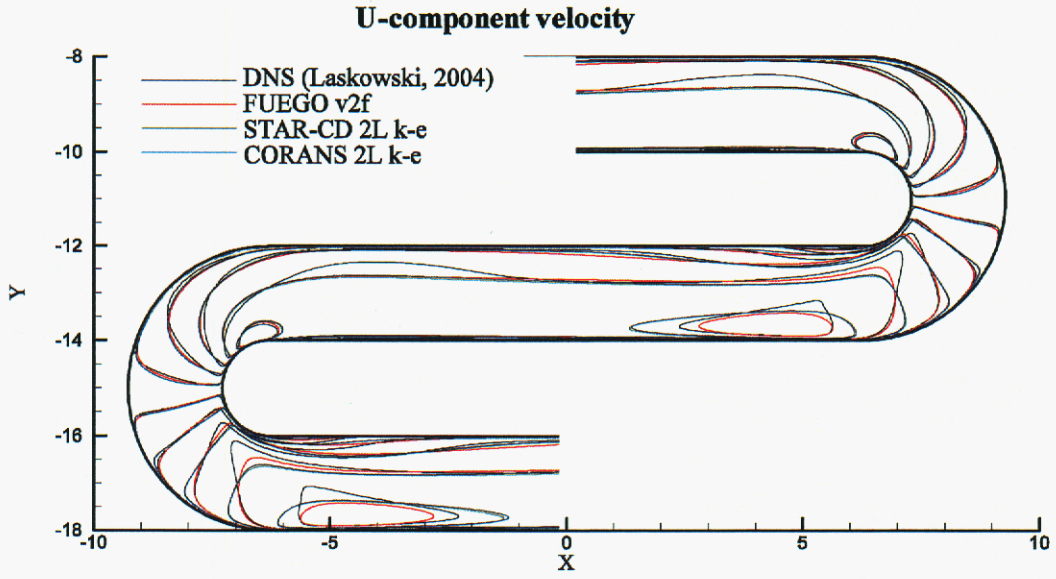

Figure 8. Comparison of Cartesian u component of velocity contours.

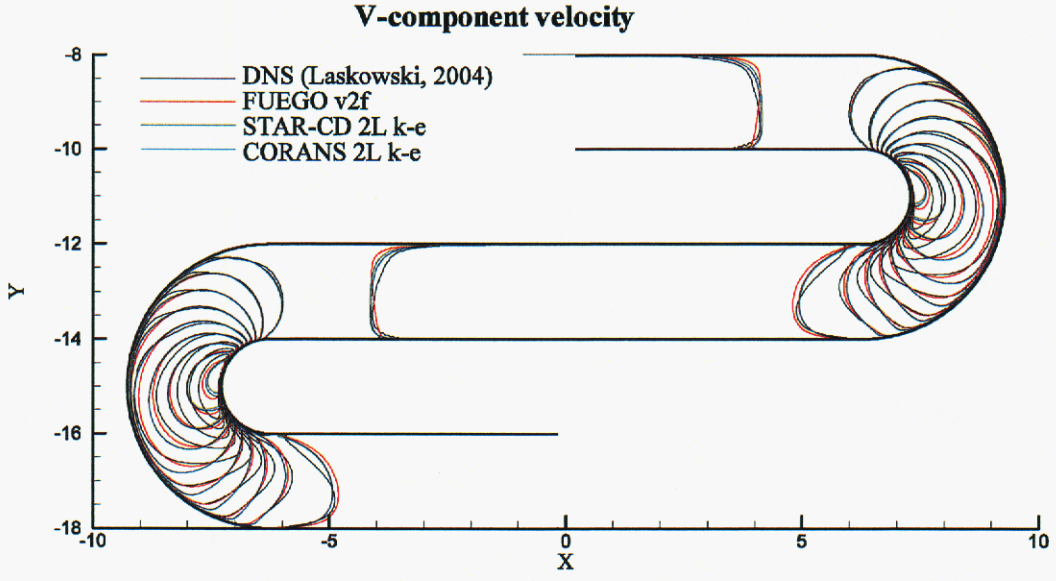

Figure 9. Comparison of Cartesian v component of velocity contours.

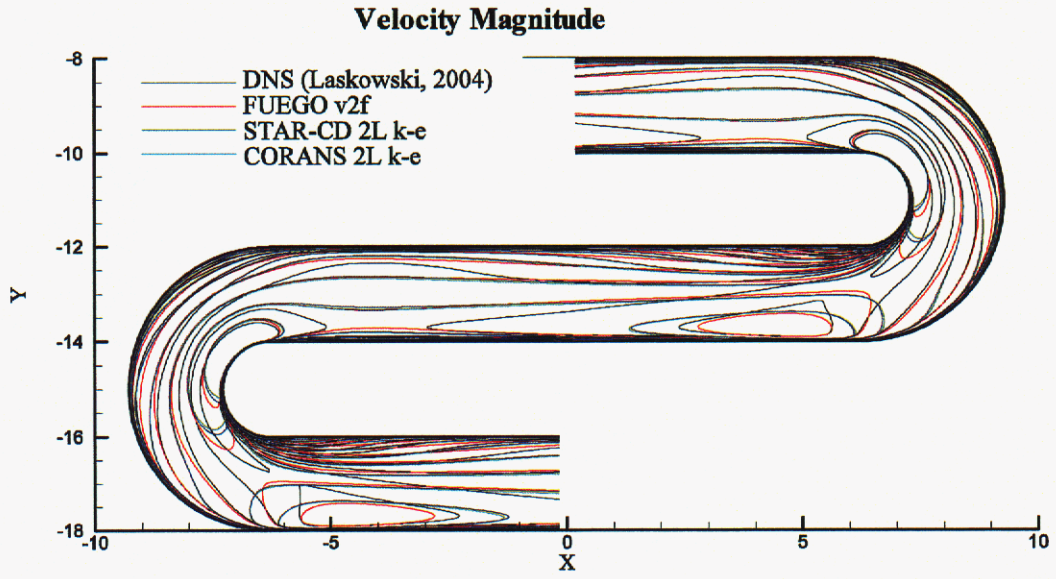

Figure 10. Comparison of velocity magnitude contours.

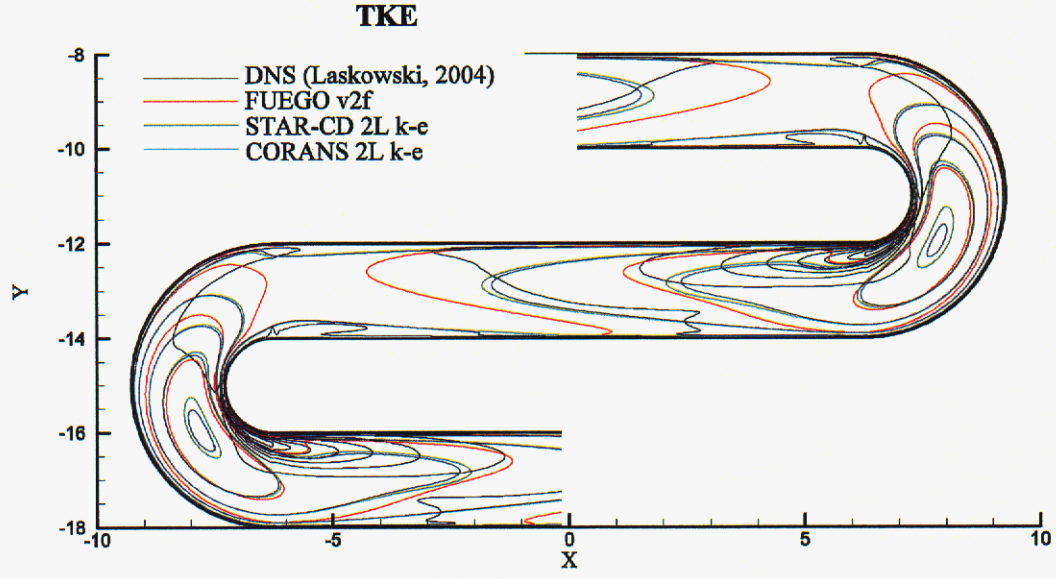

Figure 11. Comparison of turbulent kinetic energy contours.

In order to avoid clutter, the original v2f model formulation results were omitted from Figure 11. Prior to proceeding with the different model formulations of the v2f model for the serpentine passage, results for a simple channel flow are presented and compared to the DNS $Re_\tau = 180$ channel results of Laskowski (2004).

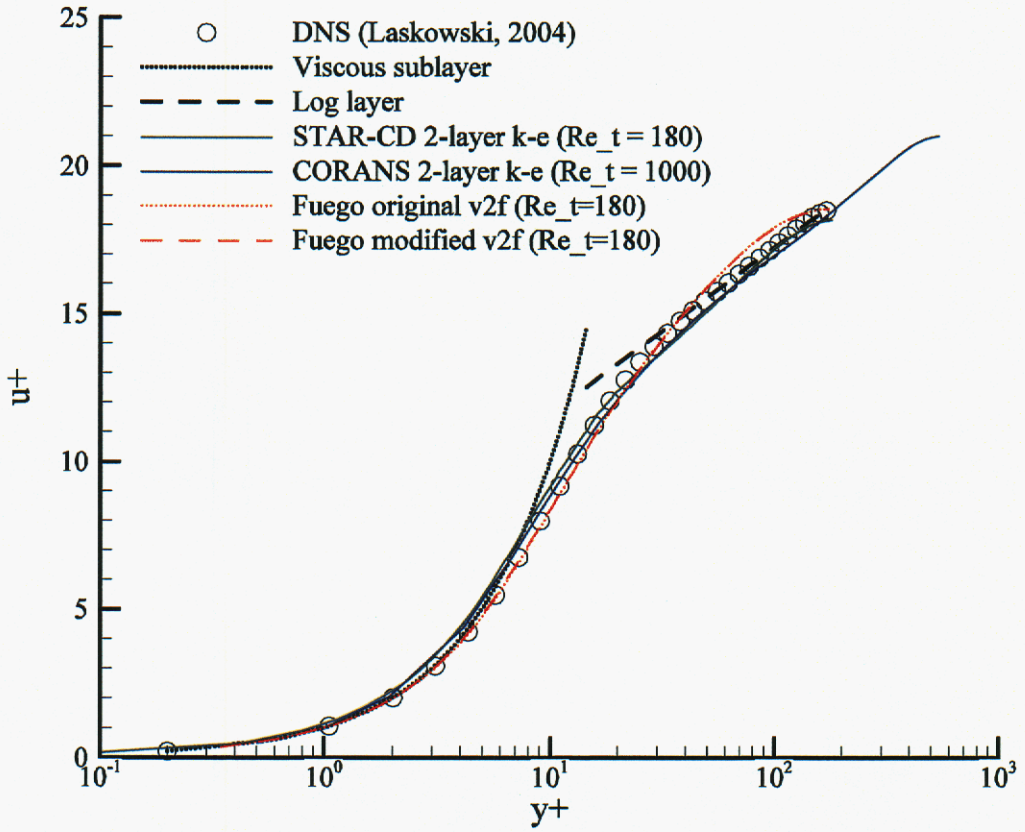

Figure 12. Original and modified v2f model channel flow velocity profile results.

Figure 12 presents the velocity profile in local wall coordinates for the modified and original v2f model. No discernable difference is noted. The models predict the viscous sublayer quite well and the transition through the buffer layer into the log layer. The extent of the log region is slightly underpredicted and this is most likely a consequence of the closure coefficients. Regardless, excellent agreement in seen between the DNS and the two model formulation of the v2f model.

Such agreement was not observed in the serpentine passage simulations. Figure 13 presents turbulent kinetic energy and velocity vector comparison between the original and modified v2f model. The modified v2f model severely over predicts separation and under predicts turbulence levels in the core of the channel. The extent of the differences can be seen in Figures 19-17.

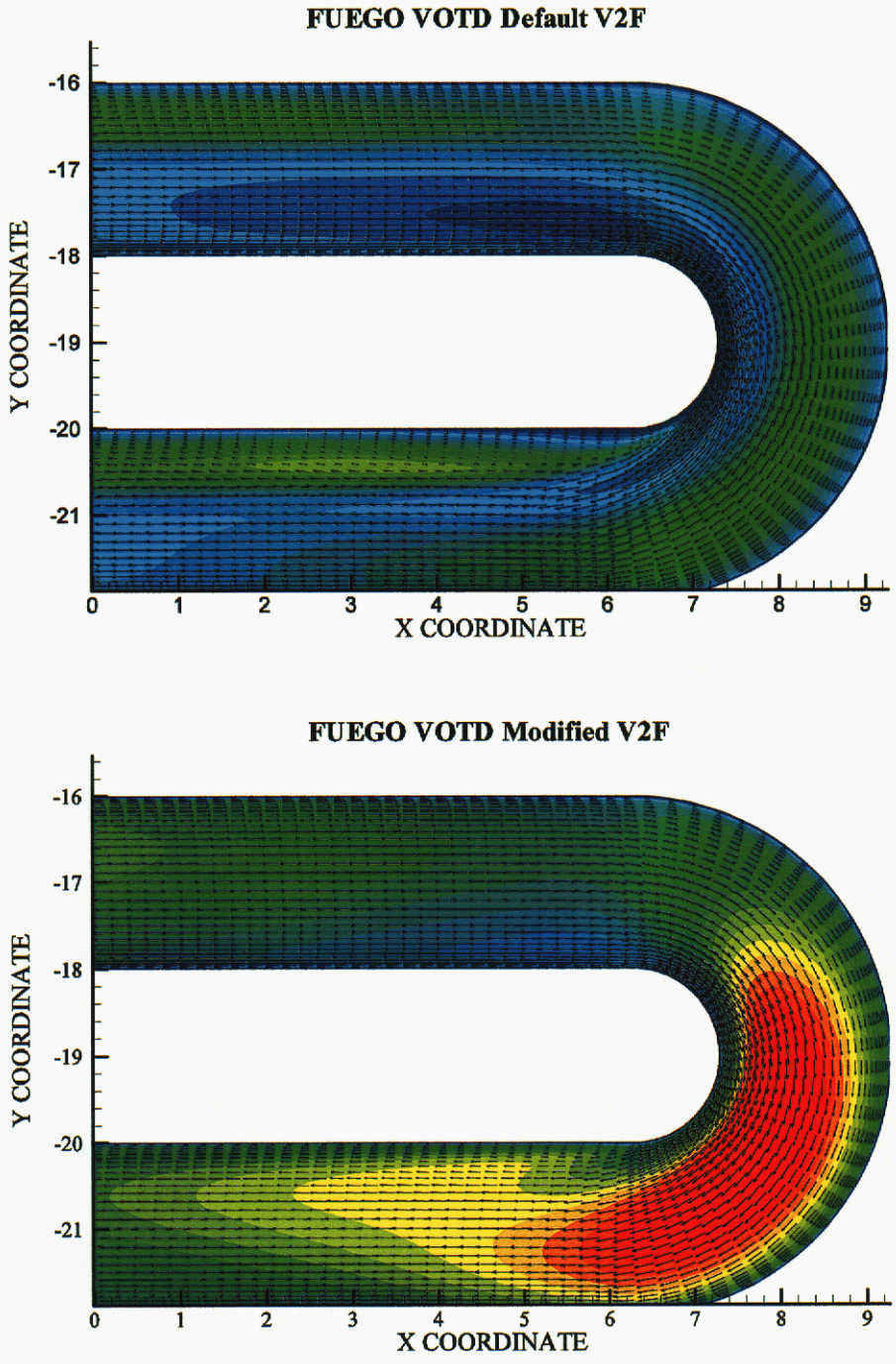

Figure 13. Turbulent kinetic energy comparison of original and modified v2f model.

Profiles for the streamwise component of velocity as well as K are plotted at the various Station locations depicted earlier in Figure 1. Figure 14 presents the streamwise velocity, *Un*, and turbulent kinetic energy, K, for Station 1, keeping in mind that Station 1 is identical to Station 5 and Station 9 due to symmetry. At Station 1 the mean flow velocity profile is asymmetric due to the curvature and periodic nature of the problem as the flow exits U-bend 2 and enters U-bend 1. The effect of the curvature is striking and bears a strong resemblance to the velocity profile observed in rotating channel flow (Kristofferson, 2003). The flow achieves a higher velocity near the inner wall than the outer wall, and a linear profile exists in the core of the channel. Near the outer wall the original v2f model results of Case 2 are in much better agreement with the DNS in terms of K than the k-ε model results of Case 3 and Case 4.

The modified v2f model underpredicts K in the core of the channel and the velocity profile is in poor agreement with the data and other cases as well. As the flow continues to develop from Station 1 to Station 2, the flow is accelerated near the inner wall due to the strong favorable pressure gradient associated with the convex surface of the bend. Furthermore, the turbulence generated by the bend decays as the flow progresses from Station 1 to Station 2. The flow continues to accelerate near the inner wall as seen by looking at the streamwise velocity profile at Station 2 and 3. This trend is captured by Cases 1-4, however the turbulent kinetic energy is much better predicted for Case 2 than Cases 3 and 4. Along the outer wall the agreement between the original v2f and DNS simulation in terms of the turbulent kinetic energy is excellent. At Station 2 the wall shear has decreased along the outer wall and increased along the inner wall. This can be explained by the pressure gradient. As the flow approaches the concave surface it experiences a favorable pressure gradient whereas the converse is true as the flow approaches the convex surface.

As the flow continues to Station 3, the momentum of the flow is insufficient to overcome the strong adverse pressure gradient that exists and separates along the convex surface well into the bend which can be seen by looking at the profiles at Station 4. Strong deviations in terms of the mean flow and variance can be seen at Station 3. Neither model is capable of predicting the high values of k associated with the *onset* of separation as the boundary layer thickens. Furthermore, the values of turbulence predicted in the core of the channel for all three cases are overpredicted by as much as a factor of two. The extent of separation is evident when looking at the profiles at Station 4. The inability of the models to capture the extent of separation reported by the DNS simulation is clearly evident. It is curious that the modified v2f model agrees much better in terms of the separation height, but severely underpredicts the turbulent kinetic energy there. Since it is the turbulent viscosity that is fed directly back into the Navier-Stokes equations, and a lower turbulent viscosity corresponds

to larger separation region, the value of turbulent viscosity in the separation region seems reasonable for the modified v2f model results. However, since K is severely underpredicted, this suggests that the dissipation is too large. Since the only difference between the modified and original v2f model results concerns the treatment of the turbulent time scale, it can be concluded that the differences is attributed to how this value is defined. Regardless, it is interesting to note that the v2f continually yields very good agreement near the outer wall which is a strong function of concave curvature, yet does not offer much improvement in terms of the inner, or convex wall when compared to the k-ε results. The former is to be expected since this is what the model was intended to improve. The later, however, is a surprise and additional studies are necessary to pinpoint the reason for this behavior.

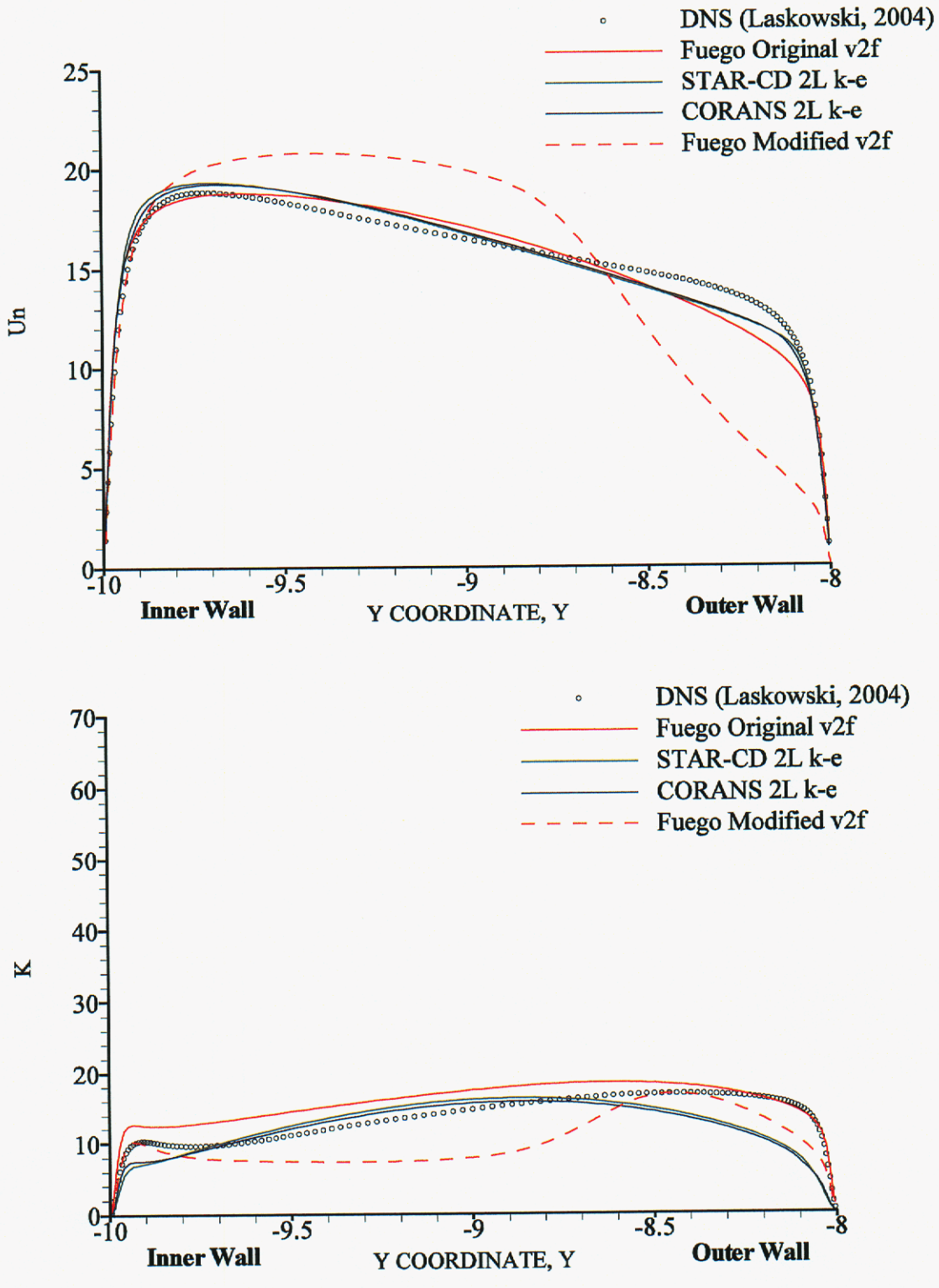

Figure 14. Streamwise velocity component and turbulent kinetic energy comparison at Station 1.

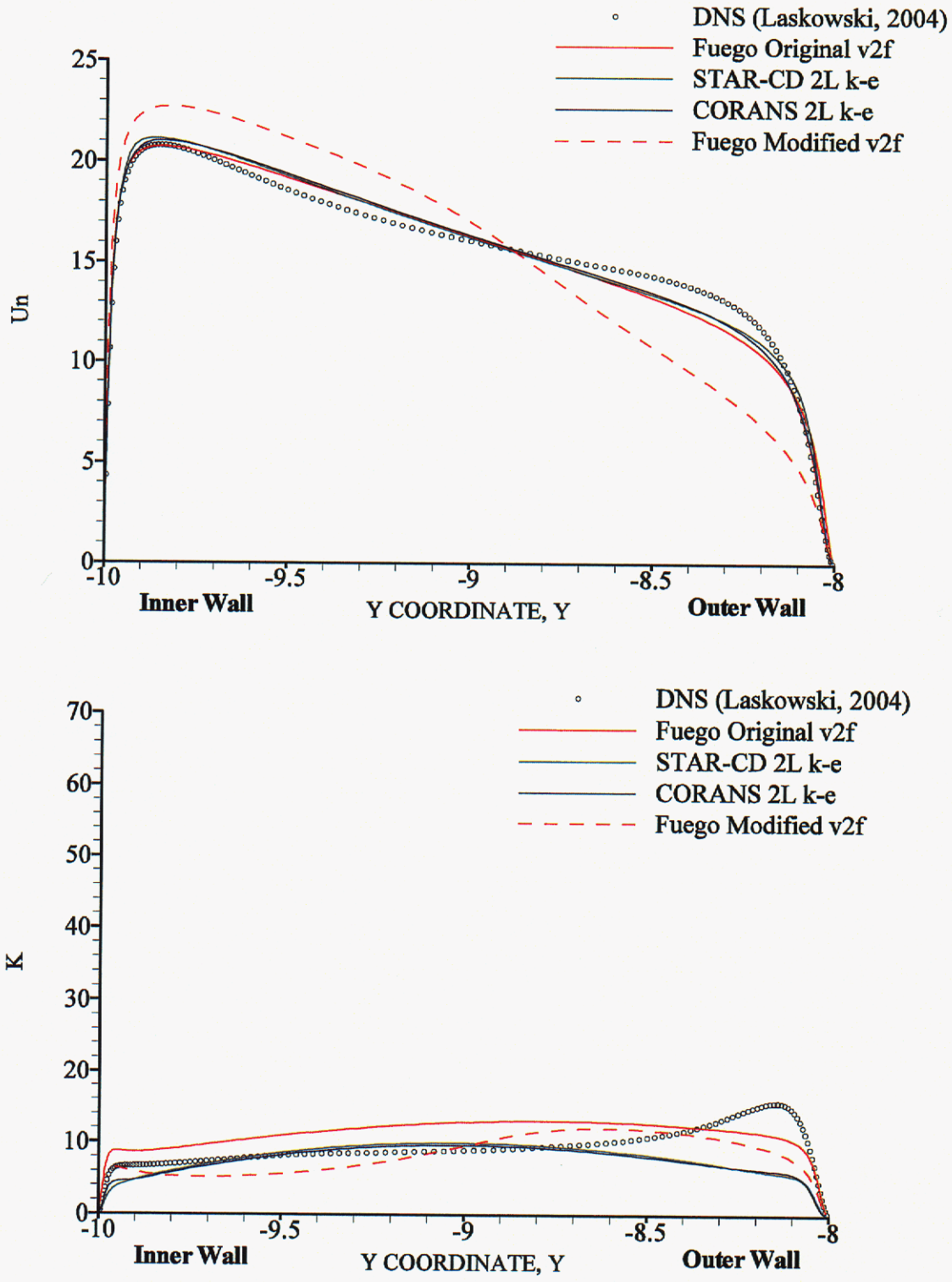

Figure 15. Streamwise velocity component and turbulent kinetic energy comparison at Station 2.

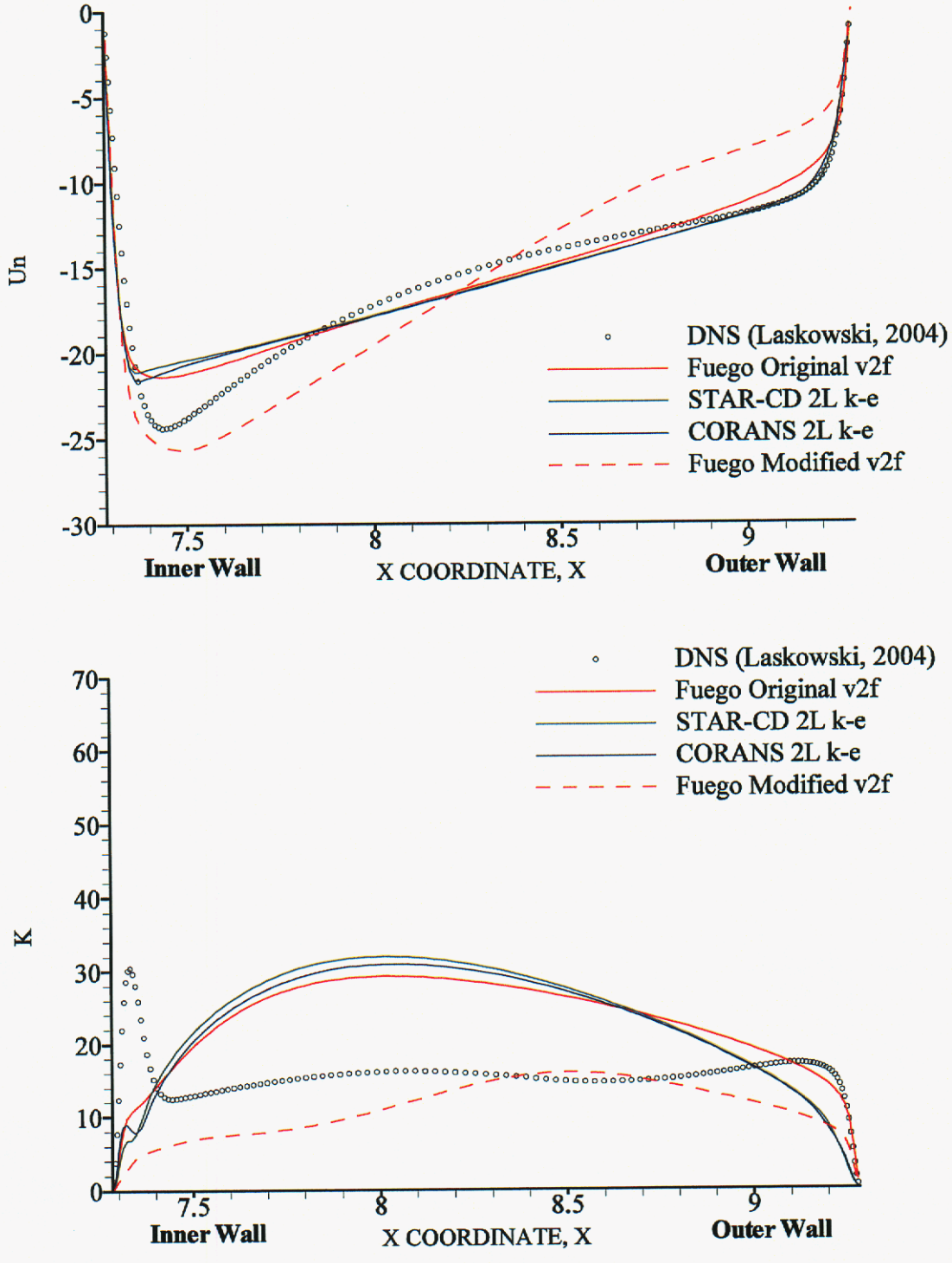

Figure 16. Streamwise velocity component and turbulent kinetic energy comparison at Station 3.

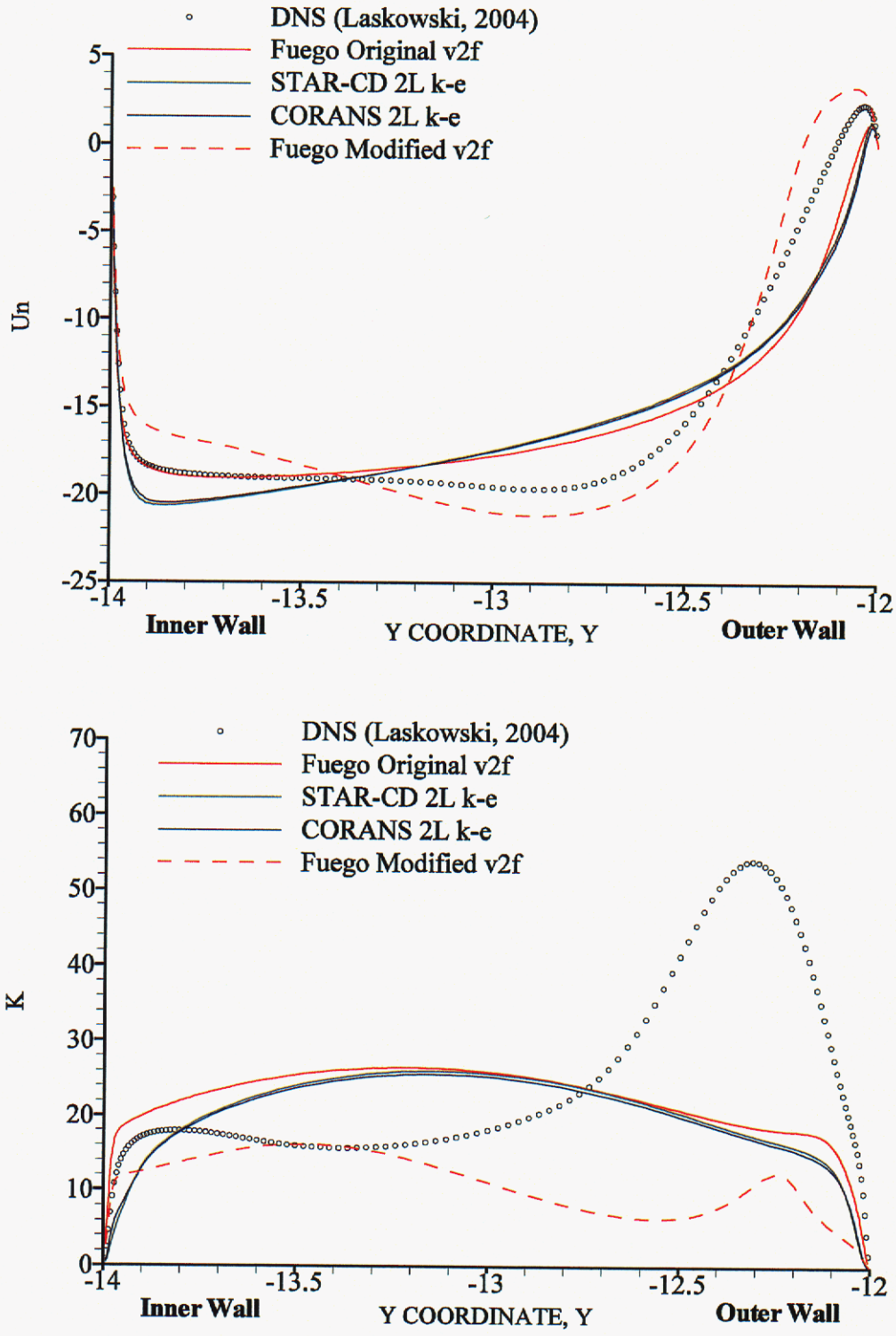

Figure 17. Streamwise velocity component and turbulent kinetic energy comparison at Station 4.

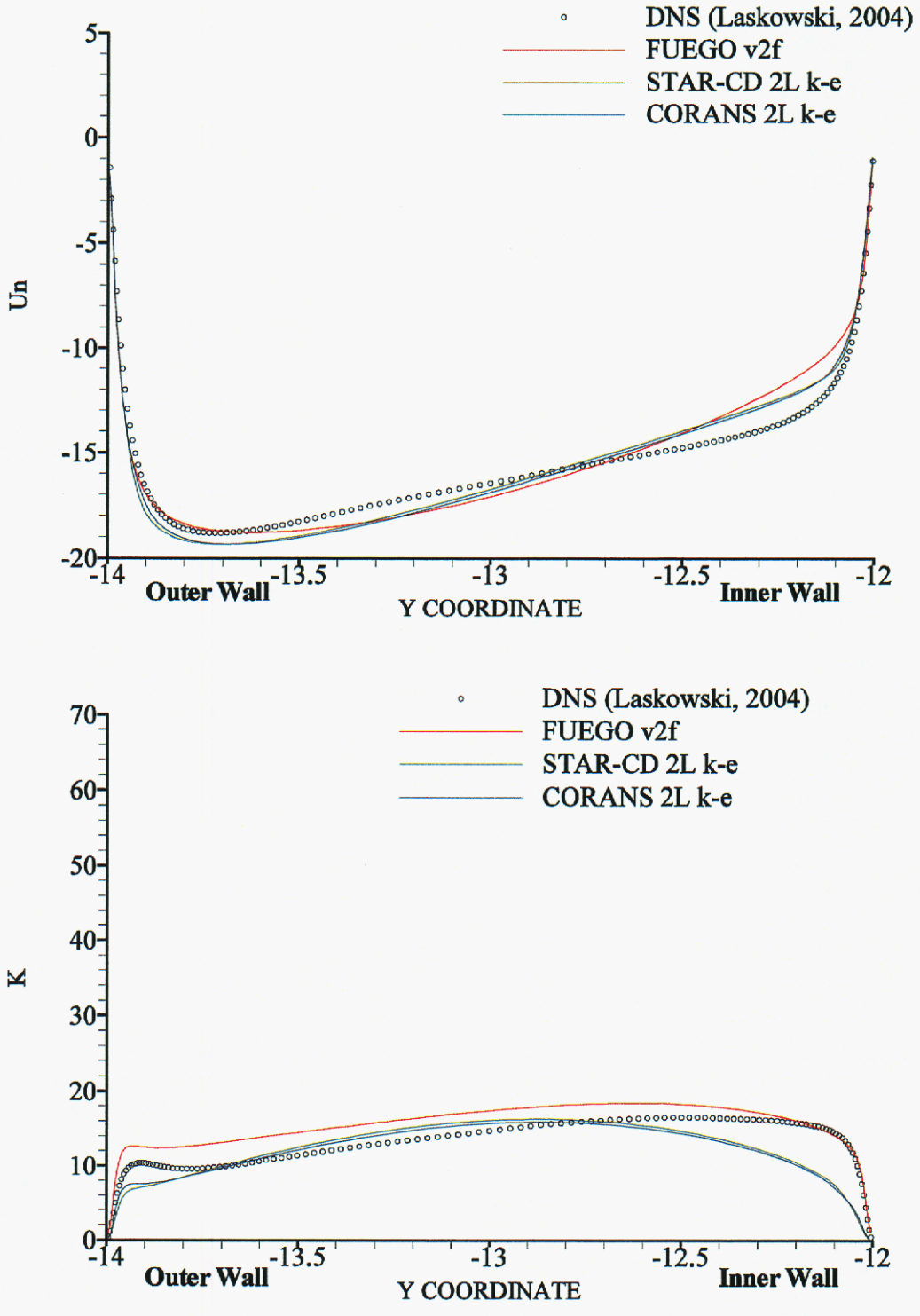

Figure 18. Streamwise velocity component and turbulent kinetic energy comparison at Station 5 (identical to Station 1).

Conclusions

Numerical simulations of flow through a stationary serpentine passage have been conducted using three different codes and two different turbulence models and the results compared to the DNS results of Laskowski (2004). Overall, the Fuego v2f simulation agreed better in terms of the mean flow and turbulent kinetic energy when compared to the CORANS and STAR-CD 2 layer k-e model simulation. Agreement between the CORANS and STAR-CD results, using the same model but different inflow/outflow boundary conditions, was excellent in terms of the third passage. The level of agreement between the DNS and RANS simulations falls of dramatically as the flow exits the straight section and enters the bend, and errors on the order of 100% in terns of the turbulent kinetic energy were observed in all cases. Such levels of agreement have been documented before in the literature for eddy viscosity type models. In order to achieve better agreement with DNS, Reynolds stress models which allow for more true anisotropy and more extensive treatment of the pressure-strain redistribution term are required.

Possible Avenues for Future Work

Two-dimensional RANS simulations were conducted to utilize the DNS data of Laskowski (2004). Three-dimensional simulations would be of interest due to the presence of secondary flow structures that were reported in the DNS study. Furthermore, it would be interesting to conduct v2f ASM simulations in both 2D and 3D to determine the level of sensitivity the model has in the bend region.

A thorough study concerning the treatment of the turbulence time and length scale treatment is required to gain confidence in results obtained with the v2f model for flows at wide ranges of Reynolds numbers[3]. It might be useful to allow the user to decide which turbulence time scale to use in each equation. For example, the user could decide to use TT or TT1 in the v2 equation.

[3] This is also for true for flows at high Rayleigh numbers where mixed and free convection are important. Currently Laskowski et al. (2005) are preparing an article for submission to the Int. J. of Heat and Fluid Flow that addresses some of these issues.

Appendix

Appendix A: Input File for SIERRA/Fuego Simulations

```
BEGIN SIERRA FUEGO

 TITLE through a serpentine

$=============================================================
$
$ Assign material properties to element blocks here.
$
$=============================================================

 BEGIN FINITE ELEMENT MODEL serpentine
  Database Name = 01/serpentine.par
  Database Type = EXODUSII

  BEGIN PARAMETERS FOR BLOCK block_1
   MATERIAL air
  END   PARAMETERS FOR BLOCK block_1
 END   FINITE ELEMENT MODEL serpentine

$=============================================================
$
$ Define the h-adaptive scheme
$
$=============================================================

$    begin uniform refinement controller my_uniform_refine_cont
$      number of outer steps = 1
$      number of inner steps = 1
$    end   uniform refinement controller my_uniform_refine_cont

$=============================================================
$
$ Define a material property set here.
$ Constant values are used to override Chemkin values.
$
$=============================================================

 BEGIN PROPERTY SPECIFICATION FOR MATERIAL air

  CHEMKIN INPUT FILE = chem.inp
  REFERENCE PRESSURE = 1.0          $ atmosphere
  REFERENCE TEMPERATURE = 288.15    $ Kelvin
  REFERENCE MOLE FRACTION N2 = 0.7905
```

```
  REFERENCE MOLE FRACTION O2 = 0.2095
  PRANDTL NUMBER = 0.72

 END PROPERTY SPECIFICATION FOR MATERIAL air


$=============================================================
$
$ Define global constants here
$
$=============================================================

 BEGIN GLOBAL CONSTANTS constants

  GRAVITY VECTOR = 0.0, -980.66, 0.0   $ cgs units
   K-E TURBULENCE MODEL PARAMETER CMU = 0.22
   K-E TURBULENCE MODEL PARAMETER SIGMA_E = 1.3
   K-E TURBULENCE MODEL PARAMETER CF_1  = 0.4
   K-E TURBULENCE MODEL PARAMETER CF_2  = 0.3
   K-E TURBULENCE MODEL PARAMETER ALPHA = 0.6
   K-E TURBULENCE MODEL PARAMETER NSEG  = 6.0
   K-E TURBULENCE MODEL PARAMETER CL    = 0.23
   K-E TURBULENCE MODEL PARAMETER CETA  = 70.0
  TURBULENCE MODEL PRANDTL NUMBER = 0.9

 END   GLOBAL CONSTANTS constants

$=============================================================
$
$ Define the functions here.
$
$=============================================================

$=============================================================
$
$ Define the linear solver parameters here.
$
$=============================================================

$ BEGIN trilinos EQUATION SOLVER continuity
$   SOLUTION METHOD = gmres
$   PRECONDITIONING METHOD = multilevel
$   PRECONDITIONING STEPS = 1
$   RESTART ITERATIONS = 50
$   MAXIMUM ITERATIONS = 250
$   RESIDUAL NORM TOLERANCE = 1.0e-5
$   RESIDUAL NORM SCALING = R0
$ END   trilinos EQUATION SOLVER continuity

 BEGIN petsc EQUATION SOLVER continuity
  SOLUTION METHOD = gmres
```

```
  PRECONDITIONING METHOD = additive-schwarz
  PRECONDITIONING STEPS = 1
  RESTART ITERATIONS = 200
  MAXIMUM ITERATIONS = 200
  RESIDUAL NORM TOLERANCE = 1.0e-5
  RESIDUAL NORM SCALING = R0
  DEBUG OUTPUT LEVEL = 0
 END   petsc EQUATION SOLVER continuity

 BEGIN aztec EQUATION SOLVER scalar
  SOLUTION METHOD = gmres
  PRECONDITIONING METHOD = symmetric-gauss-seidel
  PRECONDITIONING STEPS = 1
  RESTART ITERATIONS = 50
  MAXIMUM ITERATIONS = 200
  RESIDUAL NORM TOLERANCE = 1.0e-6
  RESIDUAL NORM SCALING = R0
  DEBUG OUTPUT LEVEL = 0
 END   aztec EQUATION SOLVER scalar

$   RESTART = automatic

$
$=============================================================
$
$ Begin the Fuego procedure (integration of equations).
$
$=============================================================

 BEGIN FUEGO PROCEDURE fuego_procedure

  TIME START = 0.0, STOP = 150.0, STATUS INTERVAL = 1


$=============================================================
$
$ Define the parameters for time integration over an interval here.
$
$=============================================================

 BEGIN TIME CONTROL

  BEGIN TIME STEPPING BLOCK  time_block

   START TIME IS   0.0
   TIME STEP = 0.001

   BEGIN PARAMETERS FOR FUEGO REGION fuego_region

    CFL LIMIT = 100.0
    TIME STEP CHANGE FACTOR = 1.1
```

```
    TRANSIENT STEP TYPE IS automatic

   END   PARAMETERS FOR FUEGO REGION fuego_region

  END   TIME STEPPING BLOCK time_block

  TERMINATION TIME IS   10000000.0

 END   TIME CONTROL

$=============================================================
$
$ Begin the Fuego region (evauation of equations within a time step).
$
$=============================================================

  BEGIN FUEGO REGION fuego_region

   USE SOLUTION STEERING WITH INTERVAL = 4

$=============================================================
$
$ Select the math model configuration for this run.
$
$=============================================================

   OPTIONS ARE fluid flow, turbulent, uniform
   NUMBER OF SPECIES = 2
   PROJECTION METHOD = fourth order SMOOTHING WITH timestep SCALING
   UPWIND METHOD IS UPW
   FIRST ORDER UPWIND FACTOR = 1.0
   TURBULENCE MODEL = v2f

   INCLUDE MOLECULAR VISCOSITY IN K-E DIFFUSION COEFFICIENT

$=============================================================
$
$ Select under relaxations for this run.
$
$=============================================================

   UNDER RELAX Momentum  by 1.0
   UNDER RELAX Pressure  by 1.0
   UNDER RELAX Turbulent Viscosity by 0.25
   UNDER RELAX Turbulence Dissipation  by 0.25
   UNDER RELAX Turbulent Kinetic Energy by 0.25
   UNDER RELAX Turbulent V2 by 0.25
   UNDER RELAX Turbulence Helmholtz Function by 0.25


$=============================================================
```

```
$
$ Select the mesh, defined at the Domain level.
$
$=============================================================

    USE FINITE ELEMENT MODEL serpentine

$=============================================================
$
$ Define the refinement scheme
$
$=============================================================

$     USE UNIFORM REFINEMENT CONTROLLER my_uniform_refine_cont

$=============================================================
$
$ Select the linear solvers for the different equation sets.
$
$=============================================================

    USE EQUATION SOLVER continuity FOR EQUATION SET Continuity
    USE EQUATION SOLVER scalar FOR EQUATION SET X-Momentum
    USE EQUATION SOLVER scalar FOR EQUATION SET Y-Momentum
    USE EQUATION SOLVER scalar FOR EQUATION SET Z-Momentum
    USE EQUATION SOLVER scalar FOR EQUATION SET Turbulent Kinetic Energy
    USE EQUATION SOLVER scalar FOR EQUATION SET Turbulence Dissipation
    USE EQUATION SOLVER scalar FOR EQUATION SET Turbulent v2
    USE EQUATION SOLVER scalar FOR EQUATION SET Turbulence Helmholtz
                                                        Function

$=============================================================
$
$ Define the nonlinear solver parameters.
$
$=============================================================

    NONLINEAR RESIDUAL PLOTFILE = serpentine.res
    MINIMUM NUMBER OF NONLINEAR ITERATIONS = 1
    MAXIMUM NUMBER OF NONLINEAR ITERATIONS = 5
    FIND MAXIMUM RESIDUALS


$=============================================================
$
$ Begin the definition of the contents of the plot file
$ for this region.
$
$=============================================================

    Begin Results Output Label output
```

```
    DATABASE Name = serpentine.e
    At Step 0, Increment = 5
    TITLE Flow through a serpentine

    NODAL Variables = pressure AS Pnd
    NODAL Variables = x_velocity AS Und
    NODAL Variables = y_velocity AS Vnd
    NODAL Variables = z_velocity AS Wnd

    NODAL Variables = density_nd AS RHOnd
    NODAL Variables = viscosity_nd AS MUnd

    NODAL Variables = turbulent_ke AS Knd
    NODAL Variables = turbulent_diss AS End
    NODAL Variables = turb_visc_nd AS TVnd

    NODAL Variables = turbulent_v2 AS V2nd
    NODAL Variables = turbulent_f AS Fnd

  End Results Output Label output

$=============================================================
$
$ Begin the definition of the restart file
$ for this region.
$
$=============================================================

  Begin Restart Data restart

    Input Database Name = serpentine.rsout4
    Output Database Name  = serpentine.rsout5
    At Step 100 Increment = 25

  End Restart Data restart

$=============================================================
$
$ Set the initial condition for this region.
$
$=============================================================

  Begin Initial Condition Block blah

    volume is block_1

    pressure = 0.0
    x-velocity = 0.0
    y-velocity = 0.0
    z-velocity = 0.0
```

```
    temperature = 288.15

    turbulent kinetic energy = 7067.
    turbulence dissipation = 352000.
    turbulence v2 = 2355.6667
    turbulence helmholtz function = 500.

  End Initial Condition Block blah


$=============================================================
$
$ Define the boundary conditions for this region.
$
$=============================================================

$ Inflow

  Begin Inflow Boundary Condition on Surface surface_1
    x-velocity = 416.1
    y-velocity = 0.0
    z-velocity = 0.0
    turbulent kinetic energy = 7067.
    turbulence dissipation = 352000.
    turbulence v2 = 2355.6667
    turbulence helmholtz function = 0.0

  End Inflow Boundary Condition on Surface surface_1

$ Outflow

  Begin Open Boundary Condition on Surface surface_3
    pressure = 0.0
    turbulent kinetic energy = 1.0e-30
    turbulence dissipation = 1.0e-30
    turbulence v2 = 1.0e-30
    turbulence helmholtz function = 1.0e-30
  End Open Boundary Condition on Surface surface_3

$ Lower surfaces (min y) are walls

  Begin wall boundary condition on surface surface_4
    turbulent kinetic energy = 1.0e-30
    turbulence v2 = 1.0e-30
    turbulence helmholtz function = 0.0
  End   wall boundary condition on surface surface_4

$ Upper surfaces (max y) are walls

  Begin wall boundary condition on surface surface_5
    turbulent kinetic energy = 1.0e-30
```

```
    turbulence v2 = 1.0e-30
    turbulence helmholtz function = 0.0
  End   wall boundary condition on surface surface_5

$ Side walls of water channel (min z); free surfaces for 2D problem.

  Begin fixed boundary condition on surface surface_2
    z-velocity = 0.0
  End fixed boundary condition on surface surface_2

$ Side walls of water channel (max z); free surfaces for 2D problem.

  Begin fixed boundary condition on surface surface_6
    z-velocity = 0.0
  End fixed boundary condition on surface surface_6

 END FUEGO REGION fuego_region
END FUEGO PROCEDURE fuego_procedure
END SIERRA FUEGO
```

References

1. Cheah, S. C., Iacovides, H., Jackson, D. C., Ji, H. and Launder, B. E. (1994) "LDA investigation of the flow development through rotating U-ducts", ASME-94-GT-226.

2. Chen, H.C. and Han, J.-C. (2002). "Computation of flow and heat transfer in turbine blade cooling passages by Reynolds stress turbulence model", *ASME FEDSM2002-31194.*

3. Chen, C.-J. and Patel, V. C., (1988) "Near-wall turbulence models for complex flows including separation", AIAA J. 26:641-648.

4. Durbin, P. A., (1991) "Near-wall turbulence closure modeling without 'damping functions", Theoret. Comput. Fluid Dynamics, 3:1-13.

5. Durbin, P. A., (1993) "Separated flow computations with the k-e-v2 model. AIAA J. 33:659-664.

6. Durbin, P. A., (2001) *Statistical Theory and Modeling for Turbulent Flows*, John Wiley & Sons Ltd.

7. Evans, G. H. (2004) Personal Communication, Sandia National Laboratories, Livermore, CA.

8. Iaccarino, G., Kalitzin, G., and Elkins, C. J. (2003). Experimental and numerical investigation of the turbulent flow in a ribbed serpentine. Annual Research Briefs, Center for Turbulence Research.

9. Iacovides, H., Launder, B. E. and Li, H-Y. (1996) The computation of flow development through stationary and rotating U-ducts of strong curvature", Int. J. Heat & Fluid Flow, 17:22-33.

10. Iacovides, H., Jackson, D. C., Kelemenis, G. and Launder, B. E. (2000) "The measurement of local wall heat transfer in stationary U-ducts of strong curvature with smooth and rib-roughened walls", J of Turbomachinery, 122:386-392.

11. Jones, W. P. and Launder, B. E., (1972) "The Prediction of laminarization with a two-equation model", Int. J. Heat Mass Transfer, 15:301-314.

12. Kenjeres, S. (1999) "Numerical Modelling of Complex Buoyancy-Driven Flows", PhD Thesis, Delft University of Technology.

13. Kristoffersen, R. and Andersson, H. J. (1993) "Direct simulations of low-Reynolds number turbulent flow in a rotating channel", J. Fluid Mechanics, 256:163-197.

14. Laskowski, G. M. (1999) "Wall Resolved LES: A First Step Towards DNS", VKI-PR 1999-0019.

15. Laskowski, G. M. (2004) "Inverse Design of a Double Passage Turbine Cascade Model and DNS of a Stationary and Rotating Serpentine Passage", PhD Thesis, Stanford University.

16. Li, H. (1995) "The computation of 3D-turbulent flows in curved and rotating ducts", PhD Thesis, UMIST.

17. Luo, J. and Lakshminarayana, B. (1997) "Prediction of strongly curved turbulent duct flows with Reynolds stress model", AIAA J. 55(1):91-98.

18. MacCormack, R. W. and Pulliam, T., (1998) "Assessment of a new numerical procedure for fluid dynamics", AIAA-98-2821.

19. Medic, G. and Durbin, P. A. (2002). "Toward improved prediction of heat transfer on turbine blades", J. of Turbomachinery, 24:187-192.

20. Moen, C. D., Evans, G. H., Domino, S. P. and Burns, S. P., (2002) "A Multi-Mechanics Approach to Computational Heat Transfer IMECE2002-33098", 2002 ASME International Mechanical Engineering Congress and Exposition, New Orleans, LA, 2002.

21. Monson, D. J., Seegmiller, H. L., McConnaughey, P. K. and Chen, Y. S. (1990) "Comparison of experiment with calculations using curvature-corrected zero and two-equation turbulence models for a two-dimensional U-duct", AIAA-90-1484.

22. Okita, Y. and Iacovides, H. (2003) "Comparisons of High-Reynolds-Number EVM and DSM models in the prediction of heat and fluid flow of turbine blade cooling passage", J. of Turbomachinery, 125:585-597.

23. Parneix, S., Durbin, P. A. and Behnia, M. (1998). "Computation of 3-D Turbulent Boundary Layers Using the V2F Model", Flow, Turbulence and Combustion, 60:19-46.

24. Rosenfeld, M., Kwak, D. and Vinokur, M. (1991) "A fractional step solution method for the unsteady incompressible Navier-Stokes equations in generalized coordinate systems", J. of Computational Physics, 94:102-137.

25. Rumsey, C. L., Gatski, T. B., and Morrison, J. H. (1999) "Turbulence model predictions of extra-strain rate effects in strongly-curved flows", AIAA-99-0157.

26. Sandborn, V. A. and Shin, J. C. (1989) "Water flow measurements ins a 180 degree turn-around duct", NASA Marshall Space Flight Center, Contract Report, June 1998.

27. Shur, M. L., Strelets, M. K., and Travin, A. K. (2000). "Turbulence modeling in rotating and curved channels: Assessing the Spalart-Shur correction", AIAA Journal, 38(5):784-792.

28. Spalart, P. R. and Allmaras, S. R. (1992) "A one-equation turbulence model for aerodynamic flows", AIAA-92-0432.

29. STAR-CD Version-3.10, (1999) *Methodology*. Computational Dynamics Ltd.

30. Svenningson, A. (2003) "Analysis of the Performance of Different v2-f Turbulence Models in a Stator Vane Passage Flow", PhD Thesis, Chalmers University of Technology.

31. Wagner, J. H., Johnson, B. V. and Kopper, F. C. (1991) "Heat transfer in rotating serpentine passages with smooth walls", J. of Turbomachinery, 112:321-330.

32. Wilcox, D. C., (2000) *Turbulence Modeling for CFD*, DCW Industries.

33. Wu, X. and Durbin, P. A., (2001) "Evidence of longitudinal vortices evolved from distorted wakes in a turbine passage", J. of Fluid Mechanics, 446:199-228.

Intentionally Left Blank

Distribution

1	MS-0382	01541	S.P. Domino
1	MS-0382	01541	S.E. Gianoulakis
1	MS-0382	01541	J.C. Sutherland
1	MS-0821	01532	L.A. Gritzo
1	MS-0828	01533	A.R. Black
1	MS-0825	01510	W.L. Hermina
1	MS-0828	01533	M. Pilch
1	MS-0834	01514	M.J. Martinez
1	MS-0836	01516	N.D. Francis
1	MS-0836	01516	E.S. Hertel
1	MS-1135	01532	A.L. Brown
1	MS-1135	01532	S.R. Tieszen
1	MS-9409	08775	G.H. Evans
3	MS-9409	08775	G.M. Laskowski
1	MS-9409	08775	C.D. Moen
1	MS-9409	08775	G.J. Wagner
2	MS-9018	08945-1	Central Technical Files
2	MS-0899	04616	Technical Library Files